HHS Public Access

Author manuscript

Cell Rep. Author manuscript; available in PMC 2022 June 22.

Published in final edited form as:

Cell Rep. 2022 June 07; 39(10): 110918. doi:10.1016/j.celrep.2022.110918.

Assembly checkpoint of the proteasome regulatory particle is activated by coordinated actions of proteasomal ATPase chaperones

Asrafun Nahar[1,3],

Vladyslava Sokolova[1,2,3],

Suganya Sekaran[1],

James D. Orth[1],

Soyeon Park[1,4,*]

[1]Department of Molecular, Cellular and Developmental Biology, University of Colorado Boulder, 1945 Colorado Avenue, Boulder, CO 80309, USA

[2]Present address: Department of Pharmacological Sciences, Stony Brook University Medical School, BST 7-120, Stony Brook, NY 117904, USA

[3]These authors contributed equally

[4]Lead contact

SUMMARY

The proteasome holoenzyme regulates the cellular proteome via degrading most proteins. In its 19-subunit regulatory particle (RP), a heterohexameric ATPase enables protein degradation by injecting protein substrates into the core peptidase. RP assembly utilizes “checkpoints,” where multiple dedicated chaperones bind to specific ATPase subunits and control the addition of other subunits. Here, we find that the RP assembly checkpoint relies on two common features of the chaperones. Individual chaperones can distinguish an RP, in which their cognate ATPase persists in the ATP-bound state. Chaperones then together modulate ATPase activity to facilitate RP subunit rearrangements for switching to an active, substrate-processing state in the resulting proteasome holoenzyme. Thus, chaperones may sense ATP binding and hydrolysis as a readout for the quality of the RP complex to generate a functional proteasome holoenzyme. Our findings provide a basis to potentially exploit the assembly checkpoints in situations with known deregulation of proteasomal ATPase chaperones.

*Correspondence: soyeon.park-1@colorado.edu.

AUTHOR CONTRIBUTIONS

Conceptualization, S.P.; methodology and investigation, A.N., V.S., S.S., and J.D.O.; writing & editing, J.D.O. and S.P.; funding acquisition, S.P.

DECLARATION OF INTERESTS

The authors declare no competing interests.

SUPPLEMENTAL INFORMATION

Supplemental information can be found online at https://doi.org/10.1016/j.celrep.2022.110918.

Graphical Abstract

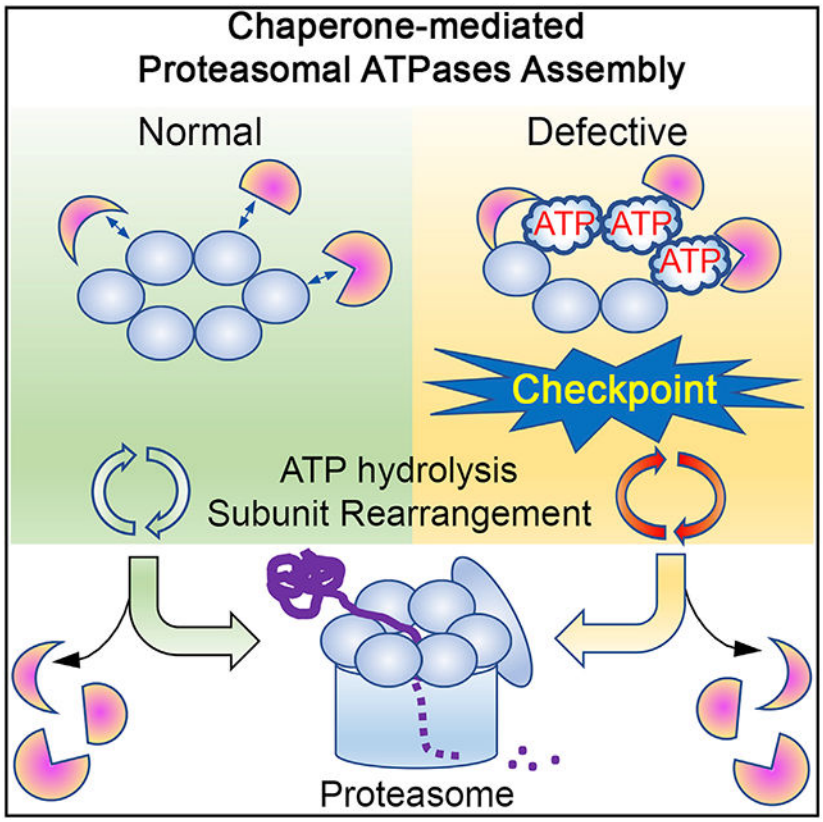

In brief

Nahar et al. report that cells build functional proteasomes by utilizing an assembly checkpoint, which is activated by a common feature of multiple dedicated chaperones; they can distinguish the nucleotide state of proteasomal ATPases and help facilitate proper subunit rearrangement to ensure efficient protein degradation by the proteasome.

INTRODUCTION

The proteasome holoenzyme is an essential protease and a central mediator of the ubiquitin-proteasome system. It maintains fundamental cellular processes by degrading numerous short-lived regulatory proteins and also ensures protein quality control by degrading aberrant or misfolded proteins (Chen et al., 2011; Hershko and Ciechanover, 1998). In the proteasome holoenzyme, the regulatory particle (RP) associates with the core particle (CP). The CP consists of seven α- and β-type subunits, which are arranged into a stack of four heteroheptameric rings ($\alpha_{1–7}\beta_{1–7}\beta_{1–7}\alpha_{1–7}$) (Groll et al., 1997). Peptidase subunits (β1, β2, and β5) are concealed in the interior of the CP and become accessible when the RP binds to the surface of the CP α ring (Groll et al., 2000). The RP is a highly dynamic structure. RP's two sub-complexes, base and lid, undergo a series of subunit rearrangements between them and also relative to the CP (Luan et al., 2016; Matyskiela et al., 2013; Sledz et al., 2013; Unverdorben et al., 2014; Wehmer et al., 2017). These changes allow the RP

base to unfold and translocate polyubiquitinated proteins into the CP for their degradation, concurrently with their ubiquitin cleavage by the RP lid. Specifically, progressive RP subunit rearrangements are coordinated by six distinct ATPases (Rpt1–Rpt6), which form a ring-shaped ATPase complex and undergo ATP hydrolysis in the RP base. This ATPase complex also anchors the RP onto the CP and induces the opening of the substrate-entry gate to activate the CP (Rabl et al., 2008; Smith et al., 2007).

To ensure efficient and accurate assembly of the RP, cells use multiple dedicated chaperones, Nas6, Rpn14, Hsm3, and Nas2, which are conserved between yeast and humans (Funakoshi et al., 2009; Kaneko et al., 2009; Le Tallec et al., 2009; Park et al., 2009; Roelofs et al., 2009; Saeki et al., 2009; Thompson et al., 2009). Specifically, chaperones act by binding to their cognate Rpt proteins, as in Nas6-Rpt3, Rpn14-Rpt6, Hsm3-Rpt1, and Nas2-Rpt5, and form three distinct modules: Rpn14-Rpt6-Rpt3-Nas6, Hsm3-Rpt1-Rpt2, and Nas2-Rpt5-Rpt4. An additional chaperone, Adc17, helps the formation of the Rpt6-Rpt3 module in yeast (Hanssum et al., 2014). Chaperones orchestrate the association of these modules into a heterohexameric ATPase ring to complete the base and then help it mature into the RP and finally into the proteasome holoenzyme. Importantly, the current model suggests that the chaperones provide “assembly checkpoints,” based on the feature that chaperones’ binding to their cognate Rpt subunits sterically hinders the addition of other subunits, until a given assembly step occurs properly (Barrault et al., 2012; Park et al., 2013; Roelofs et al., 2009; Satoh et al., 2014). A major checkpoint for RP assembly is proposed via studies on the Nas6 chaperone (Li et al., 2017; Lu et al., 2017; Nemec et al., 2019). Nas6 hinders the lid binding until completion of a heterohexameric ATPase ring of the base. The assembled base then initiates its fundamental activity, ATP hydrolysis, which relieves Nas6 hindrance and permits the lid binding to complete RP assembly. This model suggests that chaperones at the RP assembly checkpoint may ensure not only proper RP subunit addition but also its functional competence, prior to the final RP-CP association step. Upon completion of the proteasome holoenzyme, chaperones are released (Park et al., 2009, 2013; Roelofs et al., 2009).

Although it is well agreed that RP chaperones together contribute to the RP assembly checkpoint, it is poorly understood how they might regulate and activate it. The checkpoint should distinguish potentially faulty complexes to influence their fate, and this function would be disrupted if chaperones go awry. Significantly, chaperone expression levels are altered in many cancer cells and seem to affect proper protein degradation, but the underlying mechanisms remain unknown. Gankyrin, an ortholog of Nas6 in humans is an onco-protein and is overexpressed in many cancers (Higashitsuji et al., 2000, 2005; Li et al., 2018). S5b, an ortholog of Hsm3 in humans, is silenced in other cancers and can also be overexpressed in additional pathological situations (Shim et al., 2012; Tsvetkov et al., 2017). Also, evidence exists that cells may normally ensure proper RP assembly via monitoring chaperone levels. Not4, an E3 ubiquitin ligase, ubiquitinates a heterohexameric Rpt ring lacking specific chaperones, attenuating its progression to the next step in base assembly (Fu et al., 2018). Inactivating Not4 ubiquitin ligase activity alone results in only a small increase in defective proteasomes, when the chaperones are expressed at their normal levels (Fu et al., 2018). Intriguingly, Not4’s connections to RP assembly seem to extend beyond its ubiquitinating activity, since complete deletion of *NOT4* does not simply mimic a Not4 ubiquitin ligase mutant but instead results in more dramatic disruptions in RP assembly and

function; CP peptidase activity remains intact (Chen et al., 2018; Panasenko and Collart, 2011). Based on these RP-specific defects in *not4Δ* cells, we hypothesized that Not4 might have an additional connection to the RP assembly checkpoint via the chaperones.

In the present study, our findings suggest that the RP assembly checkpoint relies on two features of the chaperones. Each specific chaperone can distinguish a defective RP, based on the nucleotide state of their cognate ATPase subunit within it. Chaperones then together modulate RP's ATPase activity to help facilitate RP subunit rearrangement for switching to active, substrate-processing states in the resulting proteasome holoenzyme. Specificity of these chaperone actions depends on their limited synthesis via Not4's transcriptional activity and influences the fate of both the proteasome holoenzyme and its protein substrates, providing dual impacts on cellular protein degradation.

RESULTS

Increased proteasome assembly can result in deficient protein degradation in the cell

To investigate whether and how Not4 might influence RP assembly, in addition to its ubiquitin-mediated mechanism (Fu et al., 2018; Panasenko and Collart, 2011), we disabled Not4 activities in two ways in budding yeast, *S. cerevisiae*. We deleted the entire *NOT4* gene, termed *not4Δ*. Also, we used previously characterized *not4* point mutants, in which both RING-domain-mediated ubiquitination activity (I64A) and the RNA recognition motif (RRM) (G167A, F202A, and C244A) are disrupted (referred to as *not4-rr* henceforth) (Chen et al., 2018; Mulder et al., 2007). The *not4-rr* mutants do not affect Not4 protein abundance or the integrity of the Ccr4-Not complex, a multi-subunit regulator of transcription and translation harboring Not4 as a component (Chen et al., 2018). By using these two mutants together, we can determine whether any effect on proteasome RP assembly in *not4Δ* cells is due to Not4-dependent effects or to general disruption of Ccr4-Not.

To examine RP assembly in the proteasome holoenzyme, we employed native gels and in-gel peptidase assays using the fluorogenic peptide substrate, Leu-Leu-Val-Tyr-AMC (LLVY-AMC). Since LLVY-AMC hydrolysis requires the RP's ability to form an RP-CP complex and to subsequently open the CP gate for substrate entry into the catalytic sites, it provides a readout for these two aspects of RP assembly in the proteasome holoenzyme (Kleijnen et al., 2007; Park et al., 2011; Sokolova et al., 2015; Nahar et al., 2019). As compared with wild-type, LLVY-AMC hydrolysis is substantially increased by the proteasome holoenzymes (RP_2-CP and RP_1-CP) in both *not4Δ* and *not4-rr* cells (Figure 1Aa). Increased LLVY-AMC hydrolysis is mainly due to the increased RP-CP complex levels, as shown by immunoblotting for a representative proteasome subunit, Rpt5 (Figure 1Ab) and not some other processes that increase proteasome activity. These data suggest that RP can bind and activate CP efficiently in *not4* mutants. Increased RP-CP complex assembly is prominent when Not4 activities are completely disabled as in *not4Δ* and *not4-rr* and is mild when Not4 activity is partially disrupted (Chen et al., 2018; Fu et al., 2018).

We next examined how increased proteasome holoenzyme assembly might influence degradation of cellular ubiquitinated proteins in *not4* mutants. Unlike peptide substrates, such as LLVY-AMC, ubiquitinated proteins require RP-mediated unfolding and

translocation, prior to their degradation by the CP (Finley, 2009). In both *not4* mutants, ubiquitinated proteins accumulated, suggesting that their degradation by the proteasome holoenzyme is impaired (Figure 1B). Although RP association with CP is increased in *not4* mutants, RP cannot function properly for processing ubiquitinated proteins for degradation; CP peptidase activity is normal (Figure 1A).

We also examined whether ubiquitinated protein levels are high in *not4* mutants due to their increased synthesis, which might increase proteasome assembly indirectly. For this, we overexpressed ubiquitin in wild-type cells to elevate ubiquitin conjugate levels (Ecker et al., 1987). However, proteasome holoenzyme level and activity remain generally unaffected in ubiquitin-overexpressing cells (Figures 1C and 1D). These data support that increased ubiquitinated protein levels in the *not4* mutants (Figure 1B) are likely not due to their increased synthesis but to their deficient degradation, resulting from Not4-dependent effects on proper proteasome assembly.

Proteasome assembly is antagonistically regulated via Not4, downstream of Rpn4

Since mechanisms of proteasome assembly are crucial for generating proteasome holoenzymes at the proper level and quality, we examined a potential relationship between Not4 and two major regulators of proteasome assembly: Rpn4 and assembly chaperones (Figure 2A). The transcription factor Rpn4 is important for maintaining normal proteasome subunit gene expression (Mannhaupt et al., 1999; Xie and Varshavsky, 2001). *RPN4* is transcriptionally upregulated when cells need to raise proteasome level and activity (Ju et al., 2004; London et al., 2004).

Although *RPN4* mRNA level in *not4* mutants was increased by approximately 2-fold (Figure 2B), Rpn4 protein level was not increased, as compared with wild type (Figure 2Ca, lanes 1–3; see quantification in Figure 2D). Since Rpn4 protein is rapidly degraded by the assembled proteasome as a negative feedback (half-life [$t_{1/2}$] = ~2 min) (Xie and Varshavsky, 2001), we blocked proteasome activity by adding PS341, a specific proteasome inhibitor. Rpn4 protein was dramatically stabilized in all PS341-treated cells (Figures 2Ca, lanes 4–6, and 2D). These results support that the proteasome holoenzyme in *not4* mutants efficiently degrades ubiquitin-independent substrates (LLVY-AMC and Rpn4), which mainly require RP-mediated opening of the CP gate. Even when Rpn4 is stabilized and continuously increases proteasome subunit expression, proteasome complex level was only marginally increased (Figure 2Cc, compare lanes 4–6 with 1–3). This result can be explained by a tight feedback between Rpn4 and assembled proteasomes to control cellular proteasome level and activity (Xie and Varshavsky, 2001). Taken together, our data suggest that Rpn4 alone cannot explain the deregulated increase on proteasome level and activity in *not4* mutants. Rather, *RPN4* mRNA may be induced as a response to overcome proteasome stress, due to disruption of a more fundamental role of Not4 on proteasome assembly.

To examine a relationship between Not4 and Rpn4, we deleted *NOT4* and *RPN4* individually and together. Since Rpn4 contributes to maintaining the normal level of proteasome subunit gene expression (Mannhaupt et al., 1999; Xie and Varshavsky, 2001), both proteasome level and activity are decreased in *rpn4Δ* cells (Figure 2E, lane 2). In the *rpn4Δ* background, deletion of *NOT4* no longer increased proteasome level and activity

(Figure 2E, lane 4). These data suggest that Not4 requires normal proteasome subunit expression and acts downstream of Rpn4 (Figure 2A). Although *rpn4Δ* and *not4Δ* exhibit low versus high proteasome levels, respectively (Figure 2E, dotted box), both are deficient in cellular protein degradation, accumulating ubiquitinated proteins (Figure 2F, dotted box). These data demonstrate that deficient RP function in *not4Δ* cells affects degradation of ubiquitinated proteins, to a similar extent as *rpn4Δ* with reduced proteasome holoenzyme level. This defect is exacerbated in *not4Δrpn4Δ* double mutants, due to an additive effect between deficient RP function and a decrease in holoenzyme level (Figure 2F, lane 4). These data suggest that Not4 provides an antagonistic control for proper assembly of the proteasome holoenzyme, acting downstream of Rpn4.

Not4 regulates synthesis of RP assembly chaperones through their transcription

Since the apparent disruption in RP function correlates with hyperactive proteasome assembly in *not4* mutants (Figures 1 and 2), we tested whether Not4 influences the regulators of RP assembly. For this, we examined four RP assembly chaperones: Rpn14, Hsm3, Nas6, and Nas2 (Funakoshi et al., 2009; Park et al., 2009; Roelofs et al., 2009; Saeki et al., 2009). Cellular abundance of all four chaperone proteins were increased to a variable extent in *not4* mutant cells (Figure 3A); Rpn14 and Hsm3 levels were more noticeably increased than Nas6 and Nas2. Chaperone abundance is normal when Not4 activity is only partially disrupted (Figure S1A). Consistent with the stability of RP assembly chaperones, their cellular abundance is not determined by their degradation but mainly by their synthesis (Rousseau and Bertolotti, 2016). Indeed, based on qRT-PCR results, the mRNA abundance of all four chaperones is increased in both *not4* mutants (Figure 3B), suggesting that increased mRNA level contributes to increased protein level of these chaperones. Our data together indicate that Not4 may negatively influence chaperone synthesis at their mRNA level.

Not4-dependent chaperone synthesis does not involve the Rpn4 transcription factor, since chaperone abundance remained comparable between wild-type and *rpn4Δ* cells and between *not4Δ* and *not4Δrpn4Δ* cells (Figure S1B). Our data provide experimental evidence that Rpn4 is not involved in maintaining chaperone levels, consistent with an apparent lack of Rpn4-binding sites in the chaperone gene promoter (Shirozu et al., 2015).

Not4 antagonizes RP chaperone synthesis transcriptionally via its NOT module in Ccr4-Not

Since Not4 belongs to the nine-subunit Ccr4-Not complex, we examined whether Not4-involved chaperone mRNA regulation depends on Ccr4-Not (Collart, 2016; Miller and Reese, 2012). For this, we tested whether deletion of any other subunits in Ccr4-Not shows the same effect as found in *not4Δ* cells, resulting in an increase in chaperone synthesis. *NOT1* is omitted in this analysis because its deletion is lethal.

Specifically, chaperone protein abundance was increased in *not2Δ*, *not4Δ*, and *not5Δ* cells (Figure 3C, lanes 2, 4, and 5). This result suggests that regulation of chaperone synthesis might involve a common function of Not2, Not4, and Not5. These subunits together form a “NOT module,” which provides a composite binding site for RNA or protein in the Ccr4-Not complex during transcription and translation regulation (Bhaskar et al., 2013; Gupta et

al., 2016; Panasenko and Collart, 2012; Villanyi et al., 2014; Buschauer et al., 2020). This combined function of the NOT module explains a more severe deregulation on chaperone synthesis in *not2Δ* and *not5Δ* cells, since Not4 protein becomes unstable in these cells, abolishing NOT module activity (Jiang et al., 2019). In *not4Δ* cells, Not2 and Not5 remain stable and may compensate for the lack of Not4's function, explaining a comparatively weaker effect of *NOT4* deletion on chaperone abundance (Jiang et al., 2019). In addition to the NOT subunits, the Ccr4-Not complex contains an RNA deadenylase, Ccr4, which promotes RNA degradation together with its regulatory subunit, Caf1 (Tucker et al., 2001, 2002). However, deletion of either *CCR4* or *CAF1* did not result in any detectable change on chaperone protein abundance (Figure 3C, lanes 6 and 9; also see Figure S1C). This result suggests that Not4 contributes to regulating chaperone levels through NOT module activity, rather than the RNase activity of the Ccr4-Not complex.

Increased chaperone protein abundance in the NOT module mutants can be attributed to increased chaperone mRNA transcription, since mRNA levels of all four chaperones are greater in both *not2Δ* and *not5Δ*, as in *not4Δ* cells, as compared with wild-type cells (Figure 3D). Proteasome holoenzyme level and activity were specifically increased in the same set of NOT subunit mutants (Figure 3E, lanes 2, 4, and 5; see RP_2-CP and RP_1-CP). Both *not2Δ* and *not5Δ* mutants also exhibited a high level of free CP relative to the *not4Δ* mutants, suggesting a potential additional influence of the NOT module on proteasome biogenesis (Figures 3E, lanes 2 and 5 versus 4, and S1D). These results together suggest that Not4 regulates chaperone mRNA abundance transcriptionally via the NOT module.

Conditional inactivation of Ccr4-Not via anchor-away deregulates RP chaperone level

If Ccr4-Not is directly involved in antagonizing transcription of the RP chaperones, its nuclear localization is expected to be important. To test this, we used the anchor-away (AA) strategy to conditionally deplete Ccr4-Not from the nucleus (Haruki et al., 2008; Jiang et al., 2019; Villanyi et al., 2014). In this strategy, an anchor is an abundant cytoplasmic protein, Rpl13A (a ribosome subunit), which is fused to FKBP12. A target protein can be tagged with FKBP-rapamycin-binding (FRB) domain. Addition of rapamycin induces a [anchor-FKBP12]-rapamycin-[FRB-target] ternary complex, rapidly depleting the target protein from the nucleus. As a target protein, we chose Not5, since FRB-fused Not5 has already been shown to deplete the NOT module from the nucleus (Villanyi et al., 2014).

Both Rpn14 and Hsm3 proteins exhibited a gradual increase at 45 and 90 min upon addition of rapamycin (Figure 3F, lanes 4–6); Nas6 showed some increase, and Nas2 showed little to no increase. In control strains harboring Rpl13A-FKBP12 alone, chaperone levels were not increased (Figure 3F, lanes 1–3). The deregulated increase in chaperone protein levels resulted in an increase in both proteasome levels and activities, without affecting total cellular abundance of proteasome subunits (Figure S1E). These data suggest that retaining a NOT module subunit in the cytoplasm can disrupt its antagonistic control on chaperone transcription within 90 min, supporting a more direct control of Ccr4-Not on chaperone expression rather than a long-term adaptation of its subunit inactivation.

RP assembly checkpoint requires proper chaperone level for its nucleotide-dependent switch

Since our data suggest that cells limit chaperone synthesis via Not4 to ensure proper RP assembly for proteasome holoenzyme formation, we investigated whether excess chaperones might influence an "RP assembly checkpoint." This checkpoint is proposed via Nas6 action in regulating the progression of base into RP, as follows (Li et al., 2017). Nas6 may obstruct lid binding during early-stage base assembly where ATPase subunits bind ATP but cannot hydrolyze it yet (Figure 4A, top; Thompson et al., 2009). This situation can be mimicked by adding ATPγS, a non-hydrolyzable ATP analog, to the base (Li et al., 2017). Upon completion of the base, Nas6 may permit base-lid (RP) assembly since ATP hydrolysis by the assembled base can reposition the base relative to lid, relieving Nas6 hindrance against the lid (Figure 4A, bottom; see the proposed steps 1–3). Due to this nucleotide-specific feature, Nas6 pull-down yields mostly the base in an ATPγS condition and both base and base-lid in an ATP condition (Li et al., 2017). Using Nas6 pull-down, we examined whether and how this RP assembly checkpoint might be influenced by increased chaperone levels in *not4* mutants. We focused on the *not4Δ* mutants henceforth, since chaperone levels and proteasome assembly are affected comparably between *not4Δ* and *not4-rr* cells (Figures 1, 2, and 3).

Upon native gel analysis of Nas6 pull-down in ATPγS, Nas6 co-precipitated mainly with base in wild-type cells, as expected (Figure 4B, lane 1). However, this nucleotide-specific feature of Nas6 was disrupted in *not4Δ* cells, since RP was already yielded in ATPγS in addition to base (Figures 4Ba and 4Bb, lane 2). The increased RP in *not4Δ* is also in complex with other chaperones, Rpn14 and Hsm3 (Figures 4Bc and 4Bd, lane 2). The prominence of the RP in the ATPγS condition suggests that the base progresses into RP without proper nucleotide-dependent control in *not4Δ* cells.

Intriguingly, in the presence of ATP, the level of Nas6-bound RP became largely comparable between wild-type and *not4Δ* cells (Figures 4Ba and 4Bb, lanes 3 and 4). This nucleotide-dependent change in Nas6-RP level suggests that the increased RP in early-stage assembly (ATPγS condition) in *not4Δ* cells was used in late-stage assembly for generating proteasome holoenzymes (ATP condition), consistent with an increased proteasome holoenzyme level in *not4Δ* (Figure 1A). If Nas6-RP level simply reflects the cellular abundance of Nas6 as a bait for pull-down, it should be consistently higher in *not4Δ* cells than wild type, regardless of nucleotide conditions, but this is not the case (Figure 4C, ATP). Since the RP contains all integral subunits in *not4Δ* cells (Table S1), RP subunit composition can be ensured at the RP assembly checkpoint. However, base-lid interaction may occur without proper restriction at this checkpoint (Figure 4A, steps 2 and 3), increasing the progression of RP assembly in *not4Δ* cells. For all affinity purifications in Figure 4, we confirmed their specificity using an untagged control (Figures S2A-S2C), and their comparable pull-down efficiency in wild type versus each specific mutant (Figures S2D-S2G); see each corresponding panel.

We examined whether chaperone levels influence base-lid interaction, since chaperone levels remain high on the RPs in *not4Δ* cells (Figures 4Bc and 4Bd, lane 4) despite comparable RP levels between wild type and *not4Δ* in ATP condition (Figures 4Ba and 4Bb, lanes 3 and 4, and 4C, ATP). It is known that one RP complex contains one binding site for each

specific chaperone; for example, one RP contains one Rpt6 and one Rpn14 chaperone at maximum, due to a 1:1 stoichiometry between them (Barrault et al., 2012; Ehlinger et al., 2013; Nakamura et al., 2007; Satoh et al., 2014). Based on this feature, we considered that Rpn14 and Hsm3 may saturate RPs in *not4Δ* cells by binding to every single RP complex, for example (Figure 4D, ATP, *not4Δ*). Normally, these chaperones may exist in ~20% of the total cellular RPs (Figure 4D, ATP, *wt*), suggesting that a sub-stoichiometric level of Rpn14 and Hsm3 might be important for the RP assembly checkpoint. To test this idea, we used wild-type cells and overexpressed Rpn14 and Hsm3 while keeping the bait (Nas6) level constant (Figure S4A, lane 6). We then repeated Nas6 pull-down in the presence of ATPγS, in which base is normally yielded. Base and RP levels were increased when Rpn14 and Hsm3 were overexpressed (Figure 4E, lane 2), similar to the results in *not4Δ* in the ATPγS condition (Figure 4B, lane 2).

To verify the results using ATPγS, we fixed specific Rpt proteins in an ATP-bound state by using *rpt-EQ* mutants; glutamine substitution for the conserved Walker B glutamate prevents ATP hydrolysis by that Rpt protein (Eisele et al., 2018). We used *rpt6-EQ* and *rpt3-EQ*, since these two Rpt subunits in the base form a major interface with the lid (Luan et al., 2016), and specifically bind to Rpn14 and Nas6, respectively. RP level was increased in both *rpt6-EQ* and *rpt3-EQ* cells with chaperone overexpression, indicating an increase in base-lid interaction (Figure 4E, compare lane 4 with 3 and 6 with 5). Rpn14 and Hsm3 levels were increased in both Rpt6EQ- and Rpt3EQ-base, when they are overexpressed (Figures 4Ea and 4Eb, lanes 4 and 6, and S4A, lanes 8 and 10). These results suggest that excess chaperones may desensitize RP assembly process to the nucleotide state.

Each specific chaperone can distinguish the nucleotide state of their cognate ATPase subunit

Since excess chaperones saturate the base indiscriminately whether their cognate or non-cognate Rpt subunit is in the ATP-bound state (Figure 4E), we tested whether or not chaperones at their endogenous expression level act in the same manner. We first conducted Rpn14 pull-down in wild-type, *rpt6-EQ* (cognate), and *rpt3-EQ* (non-cognate) cells. Rpn14 in wild-type cells co-precipitated with base but barely with RP, supporting its transient binding to RP (Figures 4Fa, lane 1, and 4D, *wt*, ATP). Free Rpn14 was detected as a fast-migrating band (Figure 4Fa, lane 1; Rpt6 is absent at this position in Figure 4Fb). Intriguingly, free Rpn14 was not readily detectable in the *rpt6-EQ* cells, and only Rpn14-bound base was present (Figure 4Fa, lane 2). Thus, Rpn14 may recognize the ATP-bound Rpt6 with high affinity and may be released to some extent when this ATP is hydrolyzed by Rpt6. This feature of Rpn14 is specific to the nucleotide state of its cognate Rpt6 and not to the non-cognate Rpt3, since free Rpn14 exists comparably between wild-type and *rpt3-EQ* cells (Figure 4Fa, lane 4). These data suggest that Rpn14 at its proper level can distinguish the nucleotide state of its cognate Rpt6 at the RP assembly checkpoint.

Next, we tested whether Nas6 at its endogenous level can discriminate the nucleotide state of its cognate Rpt3, as proposed by experiments using ATPγS (Figure 4A; Li et al., 2017). Indeed, Nas6-RP was decreased specifically in *rpt3-EQ* and not in *rpt6-EQ* cells (Figures S2Ha and S2Hb), verifying the model that Nas6 action in ATPγS-bound base can

be attributed to the ATP-bound state of Rpt3. In *rpt3-EQ* cells, decreased Nas6-RP was accompanied with some increase in free Nas6 (Figure S2Ha, lane 2). Thus, ATP hydrolysis by Rpt3 in the RP may increase Nas6 binding affinity for the RP, allowing Nas6 to associate with RP more commonly, as compared with Rpn14 and Hsm3.

To examine whether Hsm3 can also distinguish the nucleotide state of its cognate Rpt1, *rpt1-EQ* cells are needed, but this mutation is inviable in yeast (Eisele et al., 2018). Instead, we used viable *rpt2-EQ* cells, since Hsm3 also contacts Rpt2 in the AAA^+ domain in the Rpt1-Rpt2 module, upon binding to its cognate Rpt1 (Barrault et al., 2012). Hsm3-bound base was increased in *rpt2-EQ*, with an accompanying decrease in free Hsm3 (Figure 4Ga, lane 2). This result suggests that Hsm3 affinity to the base is increased, when Rpt2 is in the ATP-bound state. This feature of Hsm3 is specifically observed in *rpt2-EQ* and not in *rpt6-EQ* cells (Figure 4Ga, lane 4). Thus, Hsm3 at its endogenous expression level can discriminate the nucleotide state of Rpt2 in the base complex.

Our findings reveal that Rpn14 and Hsm3 can distinguish the nucleotide state of their cognate ATPase within the RP base. This feature may allow chaperones to recognize an inappropriate or faulty RP since their affinity is increased for their cognate ATPase when these ATPase subunits persist in the ATP-bound state (see discussion). Chaperones may sense the nucleotide state as a real-time readout for the quality of the RP complex, since ATPase activities are influenced by its subunit positioning during base-lid interaction (Bashore et al., 2015; Beckwith et al., 2013). Nas6 can stably exist on this RP with ongoing ATP hydrolysis, preventing RP incorporation into the proteasome holoenzyme, until proper base-lid interaction is established (Li et al., 2017; Lu et al., 2017; Nemec et al., 2019). Thus, the chaperones control the RP assembly checkpoint by tightly coordinated actions, with the NOT module limiting their cellular level via transcriptional repression.

Chaperones together influence ATP hydrolysis at the RP assembly checkpoint

Our data suggest a model in which chaperones may ensure proper RP assembly at its checkpoint by recognizing the ATP-bound state of their cognate ATPase. This model prompts a question whether chaperones can influence ATP hydrolysis (Figure 4A, step 2). ATP hydrolysis is a fundamental activity of the RP base and is known to coordinate base-lid interaction to enable multi-step protein degradation in the resulting proteasome holoenzyme (Matyskiela et al., 2013; Sledz et al., 2013; Unverdorben et al., 2014). To examine whether chaperones influence the ATPase rate, we used RP, since the ATPase rate is stimulated when the base (~50 ATPs/min) matures into the RP (~100 ATPs/min) (Beckwith et al., 2013). This rate is extremely low in unassembled ATPases (Thompson et al., 2009).

All three chaperones, Nas6, Rpn14, and Hsm3, decreased RP's ATP hydrolysis to a variable extent (Figure 4H; also see Figure S3). Although Nas6 alone minimally decreased ATP hydrolysis by the RP, the addition of three chaperones (Nas6, Rpn14, and Hsm3) together decreased ATP hydrolysis by more than 50% to nearly 60 ATPs/RP/min, when they were provided at a 1-, 2.5-, and 5-fold molar ratio to the RP (Figure 4H). Increasing molar amounts of the chaperones does not cause a greater inhibitory effect, suggesting that chaperones can readily saturate their cognate Rpt subunit in the RP complex, when they are present at an equimolar ratio with RP. Hsm3 exhibits the most noticeable inhibitory

effect, likely because it binds to not only the cognate Rpt1 but also the AAA^+ domain of the neighboring Rpt2 (Barrault et al., 2012). Nas2 did not affect RP's ATPase activity, since its binding site on Rpt5 is occluded upon completion of base assembly (Figure 4H; Satoh et al., 2014; Tomko et al., 2010). In total, our data reveal that chaperones together influence ATP hydrolysis by the RP upon recognizing a potentially defective RP complex, in which their cognate ATPases persist in an ATP-bound state.

The RP assembly checkpoint facilitates subunit rearrangement for proper RP remodeling

We sought to examine whether chaperone-dependent regulation of ATP hydrolysis might facilitate proper base-lid interaction (Figure 4A, step 3). Base and lid subunits undergo progressive rearrangement from the inactive state (s1, substrate-free) to several related, active states (s2–s4, substrate-processing), as identified by structural studies of the proteasome holoenzyme (Bard et al., 2018). A conformation-selective reporter was developed to distinguish the s1 state from the s2–s4 states in the cell, using two engineered cysteines: Rpn7 (*rpn7-D123C*) in the lid and Rpt2 (*rpt2-R407C*) in the base (Eisele et al., 2018). A disulfide bond forms specifically in the s1 state, where two cysteines are proximal (Figure 5A, left), but not in the other states, where two cysteines become far apart, due to RP subunit rearrangement (Figure 5A, right). Since these four states co-exist in equilibrium, any change in the proportion of the s1 state means a corresponding change in the proportion of the other states.

To examine the proportion of the s1 state in the chaperone-bound RP pool, we used Nas6-pull-down samples (as in Figure 4B, lanes 3 and 4) and induced s1 state-selective crosslinks by adding a mild oxidant, Cu^{2+}. Crosslinks cause a band shift, due to an increase in combined molecular mass between Rpn7 and Rpt2, as compared with non-crosslinked Rpn7 (Eisele et al., 2018). During ATP hydrolysis by the RP ATPases, the s1 state was detected in ~10% of RPs in wild-type and ~20% of the chaperone-enriched RPs in *not4Δ* cells (Figures 5B and 5C, lane 2 versus 6). These data suggest that RP subunits may not readily rearrange from s1 to the other states in *not4Δ* cells, due to non-specific reduction of ATP hydrolysis by the chaperone-enriched RP. ATPγS traps the RP ATPases in an ATP-bound form without hydrolysis, increasing the s3 state with an accompanying decrease in the s1 state (Figures 5B and 5C, lanes 4 and 8); this confirms the state specificity of the s1 reporter (Eisele et al., 2018).

The proteasome holoenzyme also exhibits an increased s1 state (~40%) in *not4Δ*, as compared with wild-type cells (~20%) (Figures 5D and 5E, lane 6 versus 2), suggesting a defect in conformational switching. To test whether this defect is due to increased chaperone levels in *not4Δ* cells, we reduced chaperone levels by generating diploid *not4Δ/Δ* cells harboring one copy of each chaperone (*chaperonesΔ/+*: *rpn14Δ/+ hsm3Δ/+ nas6Δ/+*; Figure S4B). Importantly, the s1 state was decreased to ~28% when chaperone levels were reduced (Figures 5F and 5G, lane 6), suggesting that the proteasome holoenzyme can more readily switch to non-s1 states (active and substrate processing); the s1 state remains at ~40% in diploid *not4Δ/Δ* cells alone (Figures 5F and 5G, lane 2). These results support that proper chaperone levels are crucial for RP subunit rearrangement to generate proteasome holoenzymes with efficient conformational switching.

Next, we used a known mutant, *s1-mut*, with a specific RP remodeling defect (Figure S5A; Nemec et al., 2019). At the final RP-CP association step (Figure S5A), the Nas6 chaperone can normally obstruct *s1-mut* RP, resulting in an accumulation of *s1-mut* RP (Figure S5B, lane 2, arrowhead; graph) (Nemec et al., 2019); the *rpt3EQ* mutant can override Nas6's steric effect, allowing the *s1-mut* RP to proceed to RP-CP complexes, similarly as in *nas6Δ* cells (Figure S5Bb, lanes 4 and 5; graph). Notably, in *not4Δ* cells, the *s1-mut* RP also proceeded to RP-CP complexes (Figure S5Bb, lane 7; graph). This result suggests that Nas6 cannot properly obstruct such a defective RP, likely since Nas6 activity is rendered inactive due to uncoordinated chaperone actions involving Rpn14 and Hsm3 at the RP assembly checkpoint (Figures 4B-4H). Unrestricted progression of RP into RP-CP complexes is even more dramatic in the combined *not4Δrpt3EQ* cells (Figure S5C, lane 4; see also Figure S5D). Cells may restrict the final RP-CP association step using non-redundant mechanisms; Not4 limits chaperone synthesis for their coordinated actions at the RP assembly checkpoint (Figures 3, 4, and 5), and Rpt3 regulates Nas6 eviction in the resulting proteasome holoenzyme (Nemec et al., 2019).

The fate of the proteasome holoenzyme is influenced by the RP assembly checkpoint

Our data suggest that the RP assembly checkpoint ensures proper RP subunit remodeling to generate functional proteasome holoenzymes. Many studies suggest that RP remodeling also contributes to protecting the proteasome holoenzyme when cells need to adapt from nutrient-rich to nutrient-starved conditions (Bajorek et al., 2003; Laporte et al., 2008; Li et al., 2019; Marshall and Vierstra, 2018; Peters et al., 20i3). For example, during glucose starvation, the RP dissociates from CP, providing a dramatic example of RP remodeling on CP. This event protects proteasome complexes from autophagy by facilitating their storage into one or two cytoplasmic foci, referred to as a proteasome storage granule (PSG) (Laporte et al., 2008; Marshall and Vierstra, 2018; Peters et al., 2013). Since the RP assembly checkpoint ensures proper RP remodeling for the proteasome holoenzyme (Figures 4, 5, and S5), we examined whether it could affect the long-term fate of the proteasome holoenzyme during glucose starvation. For this, we tracked GFP-tagged Rpt6, Rpn5, and Pre10 as representative subunits of base, lid, and CP, respectively, using live-cell microscopy.

Normally, proteasome holoenzymes are localized prominently in the nucleus and diffusely in the cytoplasm when cells are grown in the presence of normal, 2% glucose (Figures 6Aa-6Ac; Isono et al., 2007; Russell et al., 1999). Upon glucose starvation, proteasomes in wild-type cells dramatically re-localize into PSGs in the cytoplasm (Figures 6Ad-6Af, arrowheads; Laporte et al., 2008; Marshall and Vierstra, 2018; Peters et al., 2013). In normal growth media, proteasome localization in *not4Δ* cells is indistinguishable from wild type (Figures 6Ag-6Ai). However, upon glucose starvation in *not4Δ* cells, PSG formation was substantially reduced compared with wild type (Figures 6Aj-6Al; see percentage of cells showing PSGs in the respective image panel). Base, lid, and CP remained largely in the nucleus. The lid in *not4Δ* cells exhibited some PSGs, since the base is mainly responsible for RP remodeling on CP (Figure 4) and its defect may disrupt PSG formation for both base and CP. In *not4-L35A* mutants, PSGs form normally (Figure S6A). To test whether impaired PSG formation in *not4Δ* cells is due to increased chaperone levels, we reduced chaperone levels (*chaperonesΔ/+*) using diploid *not4Δ/Δ* cells. Indeed, PSG formation was

largely restored (Figures 6Am-6Ao), as can be explained by restored RP remodeling via chaperones at more normal levels (Figures 5F and 5G).

We tested whether excess chaperones in *not4Δ* cells might exclude RPs from incorporating into PSGs. If so, chaperones should co-localize with RPs in the nucleus. However, chaperones localized diffusely throughout nucleus and cytoplasm in both wild-type and *not4Δ* cells (Figure S6B), clarifying that they do not directly mediate RP incorporation into PSGs. Consistent with the current model, chaperones facilitate *de novo* RP assembly for the proteasome holoenzyme. The long-term fate of the proteasome holoenzyme can be influenced by the RP assembly checkpoint during its *de novo* assembly via chaperones.

Since PSGs help protect proteasome complexes from autophagy during glucose starvation (Li et al., 2019; Marshall and Vierstra, 2018), we examined the fate of proteasome holoenzymes in *not4Δ* cells, using a GFP-release assay. In a GFP-fused protein, the fused protein is readily destroyed by autophagy, but the GFP moiety is resistant to such degradation, releasing as a free GFP (Li et al., 2019; Marshall and Vierstra, 2018). Free GFP was detected in all three GFP-tagged Rpt6, Rpn5, and Pre10 in *not4Δ*, as compared with wild-type cells (Figure 6B, compare lanes 2, 4, and 6 with 1, 3, and 5); such GFP release was largely blocked upon deletion of *PEP4*, a major autophagic protease (Figure 6B, lanes 8, 10, and 12). These data support that proteasome holoenzymes in *not4Δ* cells failed to re-localize into PSG and instead became more prone to autophagic degradation.

The fate of the proteasome holoenzyme depends on RP remodeling via Rpt3 and Rpt6 tails

To ascertain whether RP remodeling on CP influences the fate of the proteasome holoenzyme, we used a known mutant, *rpt3-Δ1rpt6-Δ1*, in which the last amino acid is deleted in the Rpt3 tail and Rpt6 tail (Park et al., 2009). These two Rpt tails contribute to anchoring the RP onto the CP in a manner tightly coordinated with RP remodeling on CP (Nemec et al., 2019; Park et al., 2013; Sokolova et al., 2015).

Strikingly, proteasome complexes in *rpt3-Δ1rpt6-Δ1* cells failed to form PSGs upon glucose starvation, as in *not4Δ* cells (Figures 6Cd-6Cf); their localization is normal in the presence of glucose (Figures 6Ca-6Cc). Failure to form PSGs is not due to a general defect in Rpt tail docking into the CP, since PSGs formed normally in both *rpt1-Δ1rpt2-Δ1* and *rpt4-Δ1rpt5-Δ1* cells to the same extent as starved wild-type cells (Figures 6Dd-6Df and 6Dj-6Dl). Proteasomal complexes become more prone to autophagic degradation specifically in *rpt3-Δ1rpt6-Δ1* cells, based on GFP-release assays (Figures S6C and S6D). Our data demonstrate that Rpt3 and Rpt6 tails have a key contribution to RP remodeling at the RP-CP interface and suggest that the RP remodeling defect on CP in *not4Δ* cells might involve these two ATPase subunits. In fact, their cognate chaperones, Nas6 and Rpn14, respectively, are key to ensuring a proper RP assembly checkpoint (Figures 4 and S5). Thus, a proper RP assembly checkpoint ensures RP remodeling, not only for protein degradation by the proteasome holoenzyme but also for the fate of the proteasome holoenzyme during nutritional stress.

DISCUSSION

Multiple dedicated RP chaperones order the sequence of RP assembly events and prevent formation of defective complexes to efficiently and accurately generate proteasome holoenzymes. Several assembly checkpoints were proposed, based on the feature that RP chaperones' binding to their cognate ATPases can block further addition of subunits until a given assembly event occurs properly (Barrault et al., 2012; Park et al., 2013; Roelofs et al., 2009; Satoh et al., 2014). However, this feature alone cannot explain whether and how chaperones might recognize inappropriate complexes and rectify them. Proper RP assembly depends on not only its subunit composition but also its subunit rearrangement to generate functional proteasome holoenzymes (Li et al., 2017; Lu et al., 2017; Nemec et al., 2019). Here, our findings suggest that the chaperones can distinguish a defective RP, based on the nucleotide state of their cognate ATPase within it, and influence their ATP hydrolysis to facilitate RP subunit rearrangement, so that only the proper RP may complete the proteasome holoenzyme.

Our findings help rationalize several aspects at the RP assembly checkpoint as to how it may ensure proper RP subunit rearrangement. In a previous study on gankyrin (a human ortholog of Nas6), gankyrin-bound RP adopts seven different conformations, and only one conformation is compatible with CP association (Lu et al., 2017). Until this one RP conformation spontaneously occurs, gankyrin is proposed to hinder the RP from associating with the CP. Here, our findings suggest that the other chaperones, Rpn14 and Hsm3, may help facilitate Nas6-bound RP remodeling by influencing its ATP hydrolysis (Figure 4H). In this way, RP might adopt a proper conformation more readily, avoiding undesirable conformations. This view is supported by the ability of Rpn14 and Hsm3 to distinguish an RP base complex, in which their cognate Rpt protein is in the ATP-bound state (Figures 4F and 4G). A prolonged ATP-bound state would occur mainly in inappropriate RP complexes, since ATP is robustly hydrolyzed when the base proceeds properly to RP assembly (Beckwith et al., 2013; Thompson et al., 2009). Co-crystal structures of each specific chaperone: Rpt complex show that the chaperone binds to the external face of the AAA^+ small domain of the Rpt protein (Ehlinger et al., 2013; Nakamura et al., 2007; Satoh et al., 2014; Takagi et al., 2012). Intriguingly, based on proteasome structures, the surface area of the AAA^+ small domain finely increases or decreases due to nucleotide-dependent positioning of the AAA^+ small versus large domain in a given Rpt protein (Beckwith et al., 2013; Sledz et al., 2013). This feature may alter chaperone binding affinity to its cognate Rpt subunit, enabling discrimination of their nucleotide state.

Our findings suggest that the RP assembly checkpoint can be impaired when chaperone expression is deregulated and might potentially be used to target some cancer cells overexpressing gankyrin or silencing S5b (an ortholog of Hsm3) (Higashitsuji et al., 2000, 2005; Tsvetkov et al., 2017). The RP assembly checkpoint helps ensure that functionally proper RP-CP complexes form during normal growth conditions (Figures 4, 5, and S5) and that they also survive through nutrient-starved conditions (Figure 6), as occurs in natural cell environments and human pathologies. The latter effect connects with an important regulatory mechanism that determines whether to protect these complexes by PSGs or to destroy them by autophagy during nutritional stresses (Figure 6). An impaired RP assembly

checkpoint would disrupt the fate of both the proteasome holoenzyme and its protein substrates. This phenomenon might create a further imbalance in the cellular proteome and disrupt fundamental cellular processes, for example, the cell cycle, which requires a precise control of ubiquitin-dependent and independent regulators through their degradation (Ben-Nissan and Sharon, 2014; Teixeira and Reed, 2013).

Combined with previous findings, our present study suggests a model as to how Not4 may enhance the fidelity of chaperone-mediated RP assembly via its distinct activities. First, Not4's E3 ligase activity selectively ubiquitinates a heterohexameric ATPase ring that assembles without chaperones, preventing its progression into the base (Fu et al., 2018). Second, our present findings suggest that Not4's transcriptional activity via its NOT module keeps chaperones at a limiting level for their coordinated actions, so that only the RP with proper subunit rearrangement may complete proteasome holoenzymes (Figures 4, 5, and S5). Third, the NOT module may also co-translationally regulate Rpt1-Rpt2 dimerization to enhance the accuracy of its cognate chaperone, Hsm3 (Panasenko et al., 2019). Although Not4 is not an RP chaperone, its distinct activities explain how Not4 may potently regulate proteasome holoenzyme assembly via the chaperones. In the cell, proteasome holoenzymes robustly assemble through many different assembly intermediates. Throughout different stages of RP assembly, RP chaperones act by the same mechanism—binding to their cognate proteasomal ATPases. The chaperones may be able to satisfy different requirements for the accuracy of a given assembly event via acting with Not4 and other proteins as potential checkpoint factors (Cheng et al., 2021; Zavodszky et al., 2021), thereby providing the first point of quality control for the proteasome holoenzyme.

Limitations of the study

While this study reveals that the chaperones at the assembly checkpoint distinguish an RP, in which their cognate ATPase persists in the ATP-bound state, and regulate ATP hydrolysis to facilitate RP remodeling, a question remains how chaperone-bound ATPases influence RP subunit rearrangement. Although this aspect was examined by the s1 state-selective reporter in the present study, structural details of RP conformations remain to be determined. As this study shows that chaperone actions rely on proper cellular concentration via transcription repression through the NOT module, mechanisms and regulation of such antagonism need further investigation, in both normal and stressed cellular conditions, which possess different needs for proteasome level and activity.

STAR★METHODS

RESOURCE AVAILABILITY

Lead contact—Further information and requests for resources and reagents should be directed to and will be fulfilled by the lead contact, Soyeon Park (soyeon.park-1@colorado.edu).

Materials availability—All unique materials generated during this study will be made available upon request to the lead contact.

Data and code availability

- All data reported in this paper will be shared by the lead contact upon request.
- This paper does not report original code.
- Any additional information required to reanalyze the data reported in this paper will be available from the lead contact upon request.

EXPERIMENTAL MODEL AND SUBJECT DETAILS

Yeast strains and manipulations—All yeast (*Saccharomyces cerevisiae*) manipulations were conducted according to standard procedures (Guthrie and Fink, 1991). A complete list of yeast strains is provided in Table S2. Unless otherwise stated, all yeast strains were grown in YPD medium at 30°C. When selection for a plasmid was necessary, strains were grown in synthetic dropout medium lacking the appropriate auxotrophic agent at 30°C. We obtained yeast strains with chromosomal deletions of specific *RPT* subunit genes or *RPN5* covered by a *URA3*-marked plasmid bearing the corresponding wild-type allele; these strains were generated in the Tomko laboratory (Eisele et al., 2018; Nemec et al., 2019). Single mutant strains were crossed, and double mutants were obtained by sporulation and dissection. We then transformed the double mutant strains with wild-type or mutant *RPT* or *RPN5* allele on *LEU2*- or *TRP1*-marked plasmids, respectively. The *URA3*-marked plasmids were then evicted by selection on 5-fluoroorotic acid media. A complete list of plasmids is provided in Table S3.

Chromosomal *not4-rr (not4-I64A, G167A, F202A, C244A), not4-ring (not4-I64A)* and *not4-rrm (not4-G167A, F202A, C244A)* strains were constructed by integrating PCR-amplified alleles into the endogenous chromosomal locus of the *NOT4*. As templates for PCR, we used plasmids from the Collart laboratory and the Laribee laboratory. We transformed each PCR-amplified fragment into the SUB62 strain and sequence-verified their correct integration into *NOT4* locus.

To generate diploid *not4Δ/Δ* cells, we crossed two haploid *not4Δ* strains with opposite mating types. To generate diploid *not4Δ/Δ* cells that are heterozygote for each specific chaperone (*not4Δ/Δ rpn14Δ/+ hsm3Δ/+ nas6Δ/+*), we crossed a haploid *not4Δ* strain with a haploid *not4Δ rpn14Δ hsm3Δ nas6Δ* strain with opposite mating types. The crossed strains were then streaked out on YPD plates to obtain well-isolated single colonies. At least 50 single colonies were individually picked into an array on new YPD plates. To identify a diploid from this array, these candidate diploids were crossed to mating type a or alpha tester strain, since only haploid cells can mate with either of these tester strains but diploid cells cannot mate with either. We further validated the identified diploids by using PCR to ensure the absence of *NOT4* gene in the diploid *not4Δ/Δ* cells and the heterozygosity of each chaperone in the diploid *not4Δ/Δ rpn14Δ/+ hsm3Δ/+ nas6Δ/+* cells. For s1 reporter experiments (Figures 5F and 5G), the diploid cells contain the s1-reporter alleles (*rpn7-D123C* and *rpt2-R407C* for disulfide crosslinking) in both copies of each corresponding gene (Table S2; SP4389A, 4390A). For PSG experiments (Figure 6A, panel m, n, o), the diploid cells contain a GFP tag on both copies of *RPT6*, *RPN5* and *PRE10* (Table S2; SP4377A, 4381A, 4385A).

METHOD DETAILS

Biochemical reagents—Biochemical reagents used in this study are listed in Key Resources Table. At least three biological replicates were performed for all biochemical and imaging experiments. For data that require quantification, exact number of biological replicates are indicated in the corresponding Figure Legend.

Native PAGE and in-gel peptidase assays—Overnight yeast cultures were diluted to OD_{600} = 0.25 and grown to approximately OD_{600} = 2 to examine proteasome level and activity. Cells were harvested by centrifugation at 3000 x g for 5 min and were washed once with ice-cold water. Cells were frozen into liquid nitrogen in a drop-wise manner, and were ground in a mortar and pestle in the presence of liquid nitrogen. The ground cryo-powders were hydrated in the proteasome buffer (50 mM Tris-HCl [pH 7.5], 5 mM $MgCl_2$, 1 mM EDTA, 10% glycerol) supplemented with protease inhibitors and, 1 mM ATP, unless otherwise indicated, and then centrifuged at 15,000 x g twice for 15 min each in the cold room. To resolve proteasomal complexes in whole cell lysates, 50 μg of protein was loaded onto 3.5% continuous native gels. To resolve affinity-purified chaperone-bound complexes, 2.5 μg of purified material was loaded onto 3.5% discontinuous native gels containing a 2.5% stacking portion. Native gels were electrophoresed for 3 hrs at 100V in the cold room. In-gel peptidase assays were conducted using the fluorogenic peptide substrate LLVY-AMC as described previously (Elsasser et al., 2005). In Figure 3E, 0.02% SDS was added to activate free CP by denaturing its substrate-entry gate, which is otherwise closed in the free CP (Groll et al., 2000). In all other Figures, in-gel peptidase assay data without SDS are shown, since free CP is minimal in both wild-type and *not4* mutant cells (for example, as seen in Figure 3E, lane 1, 4). Native gels were photographed under UV light using Bio-Rad Gel Doc EZ Imager to detect AMC fluorescence.

SDS-PAGE and immunoblotting—Protein samples were prepared as described in Native PAGE section above, mixed with 2x Laemmli buffer, and boiled for 5 min. Twenty μg of whole cell lysates or 1 μg of affinity-purified chaperone-bound complexes was loaded onto 10% Bis-Tris SDS-PAGE gels. Electrophoresis was conducted for 1 hr at room temperature.

For immunoblotting, a SDS-PAGE gel, or a native PAGE gel was transferred to a PVDF membrane. The PVDF membrane was incubated in 20 mL blocking buffer (TBST; Tris-buffered saline containing 0.1% Tween-20) containing 5% non-fat dry milk, for 1 hr. The membrane was washed twice for 10 min each using TBST. Primary antibodies were diluted in blocking buffer, and were incubated with the membrane for 1 hr, followed by two washes using TBST as above. The HRP-conjugated secondary antibody (1:3000 dilutions in blocking buffer) was incubated with the membrane for 1 hr, followed by two washes using TBST. PVDF membranes were subjected to enhanced chemiluminescence (Perkin Elmer, Western Blot Chemiluminescence Reagents Plus) and were developed using Bio-Rad ChemiDoc MP Imager. Prior to acquiring a ChemiDoc MP Imager, immunoblots were developed using a Kodak X-OMAT processor and X-ray films (Figures 1D, 2F, 3A, and S1A).

Real-time quantitative PCR—Fifty ml cultures were prepared to grow yeast cells to exponential phase. One μg of total RNA was reverse transcribed to cDNA in 20 μL reactions with oligo-dT primer and a reverse transcriptase (IMPROM-II, Promega, PRA3802). Real-time RT-PCR was performed using IQ SYBR Green Supermix (Bio-Rad, 1708882) according to manufacturer instructions. Quantitative RT-PCR results for *RPN4* and the chaperone genes (*RPN14*, *HSM3*, *NAS6*, *NAS2*) are normalized to a control gene, *ACT1*, and their fold induction in each specific mutant is calculated relative to wild type. See Key Resources Table for primers.

Affinity-purification of chaperone-bound assembly intermediates—To isolate chaperone-bound complexes, 3xFLAG affinity-tag is appended to individual chaperones in their endogenous chromosomal locus. Yeast cultures (300 mL) were grown to OD_{600} = 2 and were harvested by centrifugation at 3000 x *g* for 5 min. Cell pellets were washed once with cold water, frozen in liquid nitrogen, and ground with mortar and pestle in the presence of liquid nitrogen. The ground cryo-powders were hydrated with proteasome buffer (50 mM Tris-HCl [pH 7.5], 5 mM $MgCl_2$, 150 mM NaCl, 1 mM EDTA, 10% glycerol, and protease inhibitors). ATP was added to 1 mM in all buffers used throughout the experiments. For affinity-purification in the presence of ATPγS, we included ATPγS at 1 mM in all buffers. Whole cell extracts were hydrated for 10 min on ice, and centrifuged at 20,000 x *g* for 30 min at 4°C. The cleared lysates were incubated with 30 μL of anti-FLAG M2-agarose beads (Sigma) for 2 hrs at 4°C. The beads were washed twice with 400 μL of proteasome buffer containing 150 mM NaCl with 1 mM ATP or 0.2 mM ATPγS, and eluted with 0.2 mg/mL 3xFLAG peptides (GLP Bio) for 1 hr at 4°C.

NADH-coupled ATPase assay—We prepared an 'ATPase master mix' containing ATP (80 mM), pyruvate kinase (75 units/mL), lactic dehydrogenase (80 units/mL), phosphoenolpyruvate (100 mM), and NADH (20 mM). In parallel, a separate set of tubes were prepared, containing RP (250 nM) with or without chaperones at 1-, 2.5- and 5-fold molar ratio to the RP when all three chaperones were added together, or at an equimolar ratio with RP when each chaperone was added individually. The ATPase master mix was then added to these tubes; the resulting mixture was pipetted into a 384-well plate (UV-Star® 384-Well Microplates). We then started plate reading for 20 min at 15 sec interval at an absorbance of 340 nm.

For every NADH molecule converted to NAD+, one ATP molecule is hydrolyzed. Thus, the absorbance is directly proportional to the ATP molecules hydrolyzed. We used Beer's Law equation: absorbance (A) = extinction coefficient(e) x path-length (L) x molar concentration (c). The extinction coefficient (e) for NADH is 6220 $M^{-1}cm^{-1}$, and path-length (L) is 0.164cm^{-1} for the 384-well plate we used. Using this formula, we first converted NADH absorbance to molar concentration (nM) at each time point. We then obtained the slope (nM/sec) by plotting these NADH nM values, and finally the ATPase rate (ATP/enzyme/min) by dividing the slope values [nM of ATP/min] by the molar concentration of the enzyme (RP).

Isolation of RP for NADH-coupled ATPase assay—The RP was affinity-purified from approximately 100 mL cryolysates from the sDL133 strain harboring Rpn11-TEV-ProA (Leggett et al., 2002). Cryolysates were hydrated in the proteasome buffer (50 mM

Tris-HCl [pH 7.5], 5 mM $MgCl_2$,1 mM EDTA, 10% glycerol) supplemented with 1 mM ATP and incubated with 500 μL of IgG resin for 2 hrs at 4°C. Resin-bound complexes were washed with 20 volumes of the proteasome buffer containing 150 mM NaCl, and then incubated with 5 volumes of proteasome buffer containing 500 mM NaCl for 1 hr, followed by an additional wash with 50 volumes of the same buffer at 4°C. The resulting resin-bound RP was washed with 10 volumes of proteasome buffer, and was eluted with TEV protease at 0.1 unit/μL (ProTEV protease, Promega) in 2 volumes of the proteasome buffer by incubating at 30°C for 1 hr. The eluates were concentrated using Amicon Ultra-0.5 centrifugal filter devices (30 kDa cut-off). ATP (1 mM) was included throughout the entire purification.

Expression and purification of recombinant chaperones for NADH-coupled ATPase assay—The chaperones were expressed in *E. coli* from pGEX6P-1 derived plasmid pJR40 (GST-Nas6), pJR56 (GST-Rpn14), pJR89 (GST-Hsm3), and pSP128 (GST-Nas2); references for each plasmid is included in Table S3. For each chaperone purification, 400 mL cultures were grown to OD_{600} = 0.6 at 37°C, and were cooled to room temperature, and were induced with 0.3 mM IPTG at 18°C water bath overnight. Cells were harvested by drop-freezing into liquid nitrogen and were cyro-lysed using a mortar and pestle. The resulting cryo-powder was hydrated in 15 mL ice-cold PBS (phosphate-buffered saline) containing 10% glycerol and protease inhibitors. Once hydrated, triton X-100 was added to 0.1% final to aid the solubilization of the proteins on ice for 15 min. Lysates were cleared by centrifugation at 20,000 x g for 30 min. Cleared lysates were mixed with glutathione sepharose resin (150 μL) for 2 hrs at 4°C. The resin-bound proteins were then washed 3 times with 15 mL PBS containing 0.1% triton X-100. Chaperones were eluted by cleaving their GST tag using PreScission protease overnight at 4°C.

Conformation-selective reporter assays—Whole cell extracts were prepared in lysis buffer (50 mM HEPES pH 7.5, 150 mM NaCl, 5 mM $MgCl_2$) supplemented with 2 mM nucleotide (ATP or ATPγS). Protein concentration was adjusted to 2 μg/μL using lysis buffer. Fifty μL of lysates (=100 μg total protein) were used per crosslinking reaction. To initiate crosslinking, $CuCl_2$ was added to 250 μM final concentration for 10 min at room temperature, as described previously (Eisele et al., 2018). The crosslinking reaction was terminated by adding 20x stop buffer (200 mM N-ethylmaleimide), and was mixed with 2x non-reducing Laemmli buffer lacking β-mercaptoethanol. Samples were boiled for 5 min. Twenty μL was loaded onto 10% Bis-Tris SDS-PAGE. Crosslinking reactions of the Nas6 pulldown material were conducted in the same manner, except that 3 μg of Nas6 pulldown material was diluted into 20 μL total volume, using the lysis buffer.

Preparation of yeast cells for live-cell confocal microscopy—Cells were grown in synthetic complete media containing normal 2% glucose overnight. To image cells in normal growth condition, the overnight cultures were diluted to OD_{600} = 0.2 in 35 mL of fresh synthetic complete media containing normal 2% glucose and were grown to OD_{600} = 0.8. Total OD_{600} = 16 worth of yeast cells were harvested by centrifugation at 3000 x g for 2 min. Cell pellets were washed twice with 1 mL of YNB media, and then resuspended in 15 μL of YNB. Seven μL of the cell suspension was then spotted onto a glass slide with a

No. 1.5 coverslip. The glass slide was coated with a 1:1 mixture of poly-lysine (0.1%) and concanavanine A solution (2 mg/mL). Coverslips were sealed to glass slides using VaLap.

For glucose starvation experiments, the overnight cultures as above were diluted to synthetic complete media lacking glucose at OD_{600} = 0.05. Cultures were grown for 4 days at 30°C with continuous shaking (Li et al., 2019). At the end of 4 days, cells were harvested and prepared for live-cell imaging and SDS-PAGE.

Live-cell confocal imaging of yeast cells—Spinning disk confocal microscopy was performed using a Yokogawa CV1000 equipped with an Olympus 100X NA1.40 UPLSAPO WD 0.13 (mm) oil immersion objective, 50 μm Nipkow microlens disk, 488 nanometer excitation laser, and a high-resolution format Hamamatsu Photonics ImagEM X2 EM-CCD (C9100-14) camera with 1024 × 1024 pixels. The emission filter (Olympus) used was 525/50 nm (GFP). Cells were brought into focus using a 790 nm laser diode auto-focusing system and single images through the center of the cells were acquired at full camera resolution. All images for comparison were acquired with identical settings using the CV1000 software and were adjusted identically using Fiji (ImageJ) for presentation purposes. For all strains and conditions, at least ten random fields of view were imaged, representative cells are shown.

QUANTIFICATION AND STATISTICAL ANALYSES

Quantification of RP level, and RP-bound Rpn14 and Hsm3 level—We estimated relative % RP levels between wild-type and *not4Δ* cells in ATPγS vs. ATP condition (Figure 4C). Using ImageJ software, band intensities of RPs were measured using immunoblots as in Figure 4B [a] and [b] panels. To calculate relative % RP levels, we set the RP with a greater band intensity as 100%, within ATPγS vs. ATP samples individually. RP in *not4Δ* (ATPγS samples) and RPin wild-type (ATP samples) were set as 100%. We also measured band intensities for Rpn14 and Hsm3 on the RP on immunoblots as in Figure 4B [c] and [d] panels, respectively, using ImageJ software. To calculate relative % of RP-bound Rpn14 and Hsm3 levels (Figure 4D), we set the band intensity for Rpn14 and Hsm3 in *not4Δ* samples as 100%, in both ATPγS and ATP conditions, since *not4Δ* samples exhibit a consistently greater value than wild-type samples.

Quantification of band intensities in immunoblots—ImageJ software was used to measure the indicated band intensities in Figures 1B, 1D, 2D, 5C, 5E, 5G, S1B, S4B, and S5B. For each specific immunoblot, the number (n) of biological replicates used for quantification is indicated in the figure legend. The calculated mean values and standard deviation of the mean are used to generate the graphs in these figures.

Quantification of live-cell images—To quantify the percentage of PSG formation in the glucose-starved cells (Figure 6), we counted the total number of cells for individual yeast strains as follows. In Figure 6A (d, e, f), *GFP-RPT6* (351 cells), *RPN5-GFP* (313 cells), and *PRE10-GFP* (293 cells) were scored, together with the *not4Δ* cells (j, k, l) harboring *GFP-RPT6* (399 cells), *RPN5-GFP* (403 cells), and *PRE10-GFP* (325 cells). In Figure 6A (m, n, o), we scored the *chaperonesΔ/+ not4Δ/Δ* cells harboring *GFP-RPT6* (485 cells), *RPN5-GFP*

(663 cells), and *PRE10-GFP* (429 cells). In Figure 6C (d, e, f), we scored the *rpt3-Δ1rpt6-Δ1* cells harboring *GFP-RPT1* (394 cells), *RPN5-GFP* (391 cells), and *PRE10-GFP* (416 cells). In Figure 6D (d, e, f), we scored the *rpt1-Δ1rpt2-Δ1* cells harboring *GFP-RPT6* (583 cells), *RPN5-GFP* (345 cells), and *PRE10-GFP* (361 cells), together with the *rpt4-Δ1rpt5-Δ1* cells in Figure 6D (j, k, l) harboring *GFP-RPT6* (445 cells), *RPN5-GFP* (409 cells), and *PRE10-GFP* (410 cells). PSG-containing cells were scored when 1 to 2 cytoplasmic foci are present. The mean percentages of PSG formation with standard deviations were calculated and are shown on the side of images in Figure 6. Representative images from at least three independent experiments were used for quantification.

Statistical analysis—Two-tailed student t-tests were conducted to obtain p values for statistical significance. Equal variance was used during the t-tests. Statistical significance was considered $p < 0.05$ and was tested by comparing the value of each specific mutant to that of wild-type. When two mutants were compared, it is indicated in the graph via a line connecting the two. Calculated mean values are depicted in graphs, and error bars indicate standard deviations. All statistics were performed using Microsoft Excel. The number of biological replicates used for the statistical analyses are indicated in each respective Figure Legend.

Supplementary Material

Refer to Web version on PubMed Central for supplementary material.

ACKNOWLEDGEMENTS

We thank Robb Tomko, Jeroen Roelofs, Dan Finley, Nick Laribee, Martine Collart, Joseph Reese, and F.C.P. Holstege for sharing reagents. All microscopy experiments were performed at the Light Microscopy Core Facility at the University of Colorado Boulder. This study was supported by R01GM127688 from the NIH (S.P.).

REFERENCES

Bajorek M, Finley D, and Glickman MH (2003). Proteasome disassembly and downregulation is correlated with viability during stationary phase. Curr. Biol 13, 1140–1144. 10.1016/s0960-9822(03)00417-2. [PubMed: 12842014]

Bard JAM, Goodall EA, Greene ER, Jonsson E, Dong KC, and Martin A (2018). Structure and function of the 26S proteasome. Annu. Rev. Biochem 87, 697–724. 10.1146/annurev-biochem-062917-011931. [PubMed: 29652515]

Barrault MB, Richet N, Godard C, Murciano B, Le Tallec B, Rousseau E, Legrand P, Charbonnier JB, Le Du MH, Guerois R, et al. (2012). Dual functions of the Hsm3 protein in chaperoning and scaffolding regulatory particle subunits during the proteasome assembly. Proc. Natl. Acad. Sci. U. S. A 109, E1001–E1010. 10.1073/pnas.1116538109. [PubMed: 22460800]

Bashore C, Dambacher CM, Goodall EA, Matyskiela ME, Lander GC, and Martin A (2015). Ubp6 deubiquitinase controls conformational dynamics and substrate degradation of the 26S proteasome. Nat. Struct. Mol. Biol 22, 712–719. 10.1038/nsmb.3075. [PubMed: 26301997]

Beckwith R, Estrin E, Worden EJ, and Martin A (2013). Reconstitution of the 26S proteasome reveals functional asymmetries in its AAA+ unfoldase. Nat. Struct. Mol. Biol 20, 1164–1172. 10.1038/nsmb.2659. [PubMed: 24013205]

Ben-Nissan G, and Sharon M (2014). Regulating the 20S proteasome ubiquitin-independent degradation pathway. Biomolecules 4, 862–884. 10.3390/biom4030862. [PubMed: 25250704]

Bhaskar V, Roudko V, Basquin J, Sharma K, Urlaub H, Seraphin B, and Conti E (2013). Structure and RNA-binding properties of the Not1-Not2-Not5 module of the yeast Ccr4-Not complex. Nat. Struct. Mol. Biol 20,1281–1288. 10.1038/nsmb.2686. [PubMed: 24121231]

Buschauer R, Matsuo Y, Sugiyama T, Chen YH, Alhusaini N, Sweet T, Ikeuchi K, Cheng J, Matsuki Y, Nobuta R, et al. (2020). The Ccr4-Not complex monitors the translating ribosome for codon optimality. Science 368, eaay6912. 10.1126/science.aay6912. [PubMed: 32299921]

Chen B, Retzlaff M, Roos T, and Frydman J (2011). Cellular strategies of protein quality control. Cold Spring Harb. Perspect. Biol 3, a004374. 10.1101/cshperspect.a004374. [PubMed: 21746797]

Chen H, Sirupangi T, Wu ZH, Johnson DL, and Laribee RN (2018). The conserved RNA recognition motif and C3H1 domain of the Not4 ubiquitin ligase regulate in vivo ligase function. Sci. Rep 8, 8163. 10.1038/s41598-018-26576-1. [PubMed: 29802328]

Cheng CL, Wong MK, and Hochstrasser M (2021). Yeast Nst1 is a novel component of P-bodies and is a specific suppressor of proteasome base assembly defects. Mol. Biol. Cell 32, ar6. 10.1091/mbc.e21-04-0178. [PubMed: 34347506]

Collart MA (2016). The Ccr4-Not complex is a key regulator of eukaryotic gene expression. Wiley Interdiscip. Rev. RNA 7, 438–454. [PubMed: 26821858]

Ecker DJ, Khan MI, Marsh J, Butt TR, and Crooke ST (1987). Chemical synthesis and expression of a cassette adapted ubiquitin gene. J. Biol. Chem 262, 3524–3527. 10.1016/s0021-9258(18)61382-1. [PubMed: 3029116]

Ehlinger A, Park S, Fahmy A, Lary JW, Cole JL, Finley D, and Walters KJ (2013). Conformational dynamics ofthe Rpt6 ATPase in proteasome assembly and Rpn14 binding. Structure 21, 753–765. 10.1016/j.str.2013.02.021. [PubMed: 23562395]

Eisele MR, Reed RG, Rudack T, Schweitzer A, Beck F, Nagy I, Pfeifer G, Plitzko JM, Baumeister W, Tomko RJ Jr., et al. (2018). Expanded coverage of the 26S proteasome conformational landscape reveals mechanisms of peptidase gating. Cell Rep. 24, 1301–1315.e5. 10.1016/j.celrep.2018.07.004. [PubMed: 30067984]

Elsasser S, Schmidt M, and Finley D (2005). Characterization of the proteasome using native gel electrophoresis. Methods Enzymol. 398, 353–363. 10.1016/s0076-6879(05)98029-4. [PubMed: 16275342]

Finley D (2009). Recognition and processing of ubiquitin-protein conjugates by the proteasome. Annu. Rev. Biochem 78, 477–513. 10.1146/annurev.biochem.78.081507.101607. [PubMed: 19489727]

Finley D, Ozkaynak E, and Varshavsky A (1987). The yeast polyubiquitin gene is essential for resistance to high temperatures, starvation, and other stresses. Cell 48, 1035–1046. 10.1016/0092-8674(87)90711-2. [PubMed: 3030556]

Fu X, Sokolova V, Webb KJ, Old W, and Park S (2018). Ubiquitin-dependent switch during assembly ofthe proteasomal ATPases mediated by Not4 ubiquitin ligase. Proc. Natl. Acad. Sci. U. S. A 115, 13246–13251. 10.1073/pnas.1805353115. [PubMed: 30530678]

Funakoshi M, Tomko RJ Jr., Kobayashi H, and Hochstrasser M (2009). Multiple assemblychaperones govern biogenesis ofthe proteasome regulatory particle base. Cell 137, 887–899. 10.1016/j.cell.2009.04.061. [PubMed: 19446322]

Ghislain M, Udvardy A, and Mann C (1993). S. cerevisiae 26S protease mutants arrest cell division in G2/metaphase. Nature 366, 358–362. 10.1038/366358a0. [PubMed: 8247132]

Groll M, Bajorek M, Kohler A, Moroder L, Rubin DM, Huber R, Glickman MH, and Finley D (2000). A gated channel into the proteasome core particle. Nat. Struct. Biol 7, 1062–1067. 10.2210/pdb1g0u/pdb. [PubMed: 11062564]

Groll M, Ditzel L, Lowe J, Stock D, Bochtler M, Bartunik HD, and Huber R (1997). Structure of 20S proteasome from yeast at 2.4 A resolution. Nature 386, 463–471. 10.1038/386463a0. [PubMed: 9087403]

Gupta I, Villanyi Z, Kassem S, Hughes C, Panasenko OO, Steinmetz LM, and Collart MA (2016). Translational capacity of a cell is determined during transcription elongation via the ccr4-not complex. Cell Rep. 15, 1782–1794. 10.1016/j.celrep.2016.04.055. [PubMed: 27184853]

Guthrie C, and Fink GR (1991). Guide to Yeast Genetics and Molecular Biology (San Diego: Academic Press).

Hanna J, Hathaway NA, Tone Y, Crosas B, Elsasser S, Kirkpatrick DS, Leggett DS, Gygi SP, King RW, and Finley D (2006). Deubiquitinating enzyme Ubp6 functions noncatalytically to delay proteasomal degradation. Cell 127, 99–111. 10.1016/j.cell.2006.07.038. [PubMed: 17018280]

Hanssum A, Zhong Z, Rousseau A, Krzyzosiak A, Sigurdardottir A, and Bertolotti A (2014). An inducible chaperone adapts proteasome assembly to stress. Mol. Cell 55, 566–577. 10.1016/j.molcel.2014.06.017. [PubMed: 25042801]

Haruki H, Nishikawa J, and Laemmli UK (2008). The anchor-away technique: rapid, conditional establishment of yeast mutant phenotypes. Mol. Cell 31, 925–932. 10.1016/j.molcel.2008.07.020. [PubMed: 18922474]

Hershko A, and Ciechanover A (1998).The ubiquitin system. Annu. Rev. Bio-chem. 67, 425–479. 10.1146/annurev.biochem.67.1.425.

Higashitsuji H, Itoh K, Nagao T, Dawson S, Nonoguchi K, Kido T, Mayer RJ, Arii S, and Fujita J (2000). Reduced stability of retinoblastoma protein by gankyrin, an oncogenic ankyrin-repeat protein overexpressed in hepatomas. Nat. Med 6, 96–99. 10.1038/71600. [PubMed: 10613832]

Higashitsuji H, Liu Y, Mayer RJ, and Fujita J (2005). The oncoprotein gankyrin negatively regulates both p53 and RB by enhancing proteasomal degradation. Cell Cycle 4, 1335–1337. 10.4161/cc.4.10.2107. [PubMed: 16177571]

Isono E, Nishihara K, Saeki Y, Yashiroda H, Kamata N, Ge L, Ueda T, Kikuchi Y, Tanaka K, Nakano A, and Toh-e A (2007). The assembly pathway of the 19S regulatory particle of the yeast 26S proteasome. Mol. Biol. Cell 18, 569–580. 10.1091/mbc.e06-07-0635. [PubMed: 17135287]

Jiang H, Wolgast M, Beebe LM, and Reese JC (2019). Ccr4-Not maintains genomic integrity by controlling the ubiquitylation and degradation of arrested RNAPII. Genes Dev. 33, 705–717. 10.1101/gad.322453.118. [PubMed: 30948432]

Ju D, Wang L, Mao X, and Xie Y (2004). Homeostatic regulation of the proteasome via an Rpn4-dependent feedback circuit. Biochem. Biophys. Res. Commun 321, 51–57. 10.1016/j.bbrc.2004.06.105. [PubMed: 15358214]

Kaneko T, Hamazaki J, Iemura S.i., Sasaki K, Furuyama K, Natsume T, Tanaka K, and Murata S (2009). Assembly pathway ofthe Mammalian proteasome base subcomplex is mediated by multiple specific chaperones. Cell 137, 914–925. 10.1016/j.cell.2009.05.008. [PubMed: 19490896]

Kleijnen MF, Roelofs J, Park S, Hathaway NA, Glickman M, King RW, and Finley D (2007). Stability of the proteasome can be regulated allosterically through engagement of its proteolytic active sites. Nat. Struct. Mol. Biol 14, 1180–1188. 10.1038/nsmb1335. [PubMed: 18026118]

Laporte D, Salin B, Daignan-Fornier B, and Sagot I (2008). Reversible cytoplasmic localization of the proteasome in quiescent yeast cells. J. Cell Biol 181, 737–745. 10.1083/jcb.200711154. [PubMed: 18504300]

Le Tallec B, Barrault MB, Guerois R, Carre T, and Peyroche A (2009). Hsm3/S5b participates in the assembly pathway of the 19S regulatory particle of the proteasome. Mol. Cell 33, 389–399. 10.1016/j.molcel.2009.01.010. [PubMed: 19217412]

Lee SYC, De la Mota-Peynado A, and Roelofs J (2011). Loss of Rpt5 protein interactions with the core particle and Nas2 protein causes the formation of faulty proteasomes that are inhibited by Ecm29 protein. J. Biol. Chem 286, 36641–36651. 10.1074/jbc.m111.280875. [PubMed: 21878651]

Leggett DS, Hanna J, Borodovsky A, Crosas B, Schmidt M, Baker RT, Walz T, Ploegh H, and Finley D (2002). Multiple associated proteins regulate proteasome structure and function. Mol. Cell 10, 495–507. 10.1016/s1097-2765(02)00638-x. [PubMed: 12408819]

Li F, Tian G, Langager D, Sokolova V, Finley D, and Park S (2017). Nucleotide-dependent switch in proteasome assembly mediated by the Nas6 chaperone. Proc. Natl. Acad. Sci. U. S. A 114, 1548–1553. 10.1073/pnas.1612922114. [PubMed: 28137839]

Li H, Zhang J, Zhen C, Yang B, and Feng L (2018). Gankyrin as a potential target for tumor therapy: evidence and perspectives. Am J Transl. Res 10, 1949–1960. [PubMed: 30093934]

Li J, Breker M, Graham M, Schuldiner M, and Hochstrasser M (2019). AMPK regulates ESCRT-dependent microautophagy of proteasomes concomitant with proteasome storage granule assembly

during glucose starvation. PLoS Genet. 15, e1008387. 10.1371/journal.pgen.1008387. [PubMed: 31738769]

London MK, Keck BI, Ramos PC, and Jürgen Dohmen R (2004). Regulatory mechanisms controlling biogenesis of ubiquitin and the proteasome. FEBS Lett. 567, 259–264. 10.1016/j.febslet.2004.04.078. [PubMed: 15178333]

Lu Y, Wu J, Dong Y, Chen S, Sun S, Ma YB, Ouyang Q, Finley D, Kirschner MW, and Mao Y (2017). Conformational landscape of the p28-bound human proteasome regulatory particle. Mol. Cell 67, 322–333.e326. 10.2210/pdb5vhj/pdb. [PubMed: 28689658]

Luan B, Huang X, Wu J, Mei Z, Wang Y, Xue X, Yan C, Wang J, Finley DJ, Shi Y, et al. (2016). Structure of an endogenous yeast 26S proteasome reveals two major conformational states. Proc. Natl. Acad. Sci. U. S. A 113, 2642–2647. 10.1073/pnas.1601561113. [PubMed: 26929360]

Mannhaupt G, Schnall R, Karpov V, Vetter I, and Feldmann H (1999). Rpn4p acts as a transcription factor by binding to PACE, a nonamer boxfound upstream of 26S proteasomal and othergenes in yeast. FEBS Lett. 450, 27–34. 10.1016/s0014-5793(99)00467-6. [PubMed: 10350051]

Marques AJ, Glanemann C, Ramos PC, and Dohmen RJ (2007). The C-terminal extension of the β7 subunit and activator complexes stabilize nascent 20 S proteasomes and promote their maturation. J. Biol. Chem 282, 34869–34876. 10.1074/jbc.m705836200. [PubMed: 17911101]

Marshall RS, and Vierstra RD (2018). Proteasome storage granules protect proteasomes from autophagic degradation upon carbon starvation. Elife 7, e34532. 10.7554/elife.34532. [PubMed: 29624167]

Matyskiela ME, Lander GC, and Martin A (2013). Conformational switching of the 26S proteasome enables substrate degradation. Nat. Struct. Mol. Biol 20, 781–788. 10.1038/nsmb.2616. [PubMed: 23770819]

Miller JE, and Reese JC (2012). Ccr4-Not complex: the control freak of eukaryotic cells. Crit. Rev. Biochem. Mol. Biol 47, 315–333. 10.3109/10409238.2012.667214. [PubMed: 22416820]

Mulder KW, Inagaki A, Cameroni E, Mousson F, Winkler GS, DeVirgilio C, Collart MA, and Timmers HTM (2007). Modulation of Ubc4p/Ubc5p-mediated stress responses by the RING-finger-dependent ubiquitin-protein ligase Not4p in Saccharomyces cerevisiae. Genetics 176, 181–192. 10.1534/genetics.106.060640. [PubMed: 17513889]

Nahar A, Fu X, Polovin G, Orth JD, and Park S (2019). Two alternative mechanisms regulate the onset of chaperone-mediated assembly of the proteasomal ATPases. J. Biol. Chem 294, 6562–6577. 10.1074/jbc.ra118.006298. [PubMed: 30814255]

Nakamura Y, Umehara T, Tanaka A, Horikoshi M, Padmanabhan B, and Yokoyama S (2007). Structural basis for the recognition between the regulatory particles Nas6 and Rpt3 of the yeast 26S proteasome. Biochem. Biophys. Res. Commun 359, 503–509. 10.1016/j.bbrc.2007.05.138. [PubMed: 17555716]

Nemec AA, Peterson AK, Warnock JL, Reed RG, and Tomko RJ Jr. (2019). An allosteric interaction network promotes conformation state-dependent eviction of the Nas6 assembly chaperone from nascent 26S proteasomes. Cell Rep. 26, 483–495.e5. 10.1016/j.celrep.2018.12.042. [PubMed: 30625330]

Panasenko OO, and Collart MA (2011). Not4 E3 ligase contributes to proteasome assembly and functional integrity in part through Ecm29. Mol. Cell Biol 31, 1610–1623. 10.1128/mcb.01210-10. [PubMed: 21321079]

Panasenko OO, and Collart MA (2012). Presence of Not5 and ubiquitinated Rps7A in polysome fractions depends upon the Not4 E3 ligase. Mol. Microbiol 83, 640–653. 10.1111/j.1365-2958.2011.07957.x. [PubMed: 22243599]

Panasenko OO, Somasekharan SP, Villanyi Z, Zagatti M, Bezrukov F, Rashpa R, Cornut J, Iqbal J, Longis M, Carl SH, et al. (2019). Co-translational assembly of proteasome subunits in NOT1-containing assemblysomes. Nat. Struct. Mol. Biol 26, 110–120. 10.1038/s41594-018-0179-5. [PubMed: 30692646]

Park S, Kim W, Tian G, Gygi SP, and Finley D (2011). Structural defects in the regulatory particle-core particle interface of the proteasome induce a novel proteasome stress response. J. Biol. Chem 286, 36652–36666. 10.1074/jbc.m111.285924. [PubMed: 21878652]

Park S, Li X, Kim HM, Singh CR, Tian G, Hoyt MA, Lovell S, Battaile KP, Zolkiewski M, Coffino P, et al. (2013). Reconfiguration of the proteasome during chaperone-mediated assembly. Nature 497, 512–516. 10.1038/nature12123. [PubMed: 23644457]

Park S, Roelofs J, Kim W, Robert J, Schmidt M, Gygi SP, and Finley D (2009). Hexameric assembly of the proteasomal ATPases istemplated through their C termini. Nature 459, 866–870. 10.1038/nature08065. [PubMed: 19412160]

Peters LZ, Hazan R, Breker M, Schuldiner M, and Ben-Aroya S (2013). Formation and dissociation of proteasome storage granules are regulated by cytosolic pH. J. Cell Biol 201, 663–671. 10.1083/jcb.201211146. [PubMed: 23690178]

Pettersen EF, Goddard TD, Huang CC, Couch GS, Greenblatt DM, Meng EC, and Ferrin TE (2004). UCSF Chimera–a visualization system for exploratory research and analysis. J. Comput. Chem 25, 1605–1612. 10.1002/jcc.20084. [PubMed: 15264254]

Rabl J, Smith DM, Yu Y, Chang SC, Goldberg AL, and Cheng Y (2008). Mechanism of gate opening in the 20S proteasome by the proteasomal ATPases. Mol Cell 30, 360–368. 10.1016/j.molcel.2008.03.004. [PubMed: 18471981]

Roelofs J, Park S, Haas W, Tian G, McAllister FE, Huo Y, Lee BH, Zhang F, Shi Y, Gygi SP, and Finley D (2009). Chaperone-mediated pathway of proteasome regulatory particle assembly. Nature 459, 861–865. 10.1038/nature08063. [PubMed: 19412159]

Rousseau A, and Bertolotti A (2016). An evolutionarily conserved pathway controls proteasome homeostasis. Nature 536, 184–189. 10.1038/nature18943. [PubMed: 27462806]

Russell SJ, Steger KA, and Johnston SA (1999). Subcellular localization, stoichiometry, and protein levels of 26S proteasome subunits in yeast. J. Biol. Chem 274, 21943–21952. 10.1074/jbc.274.31.21943. [PubMed: 10419517]

Saeki Y, Toh EA, Kudo T, Kawamura H, and Tanaka K (2009). Multiple proteasome-interacting proteins assist the assembly of the yeast 19S regulatory particle. Cell 137, 900–913. 10.1016/j.cell.2009.05.005. [PubMed: 19446323]

Satoh T, Saeki Y, Hiromoto T, Wang YH, Uekusa Y, Yagi H, Yoshihara H, Yagi-Utsumi M, Mizushima T, Tanaka K, and Kato K (2014). Structural basis for proteasome formation controlled by an assembly chaperone nas2. Structure 22, 731–743. 10.1016/j.str.2014.02.014. [PubMed: 24685148]

Schneider CA, Rasband WS, and Eliceiri KW (2012). NIH Image to ImageJ: 25 years of image analysis. Nat. Methods 9, 671–675. 10.1038/nmeth.2089. [PubMed: 22930834]

Shi Y, Chen X, Elsasser S, Stocks BB, Tian G, Lee BH, Shi Y, Zhang N, de Poot SAH, Tuebing F, et al. (2016). Rpn1 provides adjacent receptor sites for substrate binding and deubiquitination by the proteasome. Science 351, aad9421. 10.1126/science.aad9421. [PubMed: 26912900]

Shim SM, Lee WJ, Kim Y, Chang JW, Song S, and Jung YK (2012). Role of S5b/PSMD5 in proteasome inhibition caused by TNF-α/NFκB in higher eukaryotes. Cell Rep. 2, 603–615. 10.1016/j.celrep.2012.07.013. [PubMed: 22921402]

Shirozu R, Yashiroda H, and Murata S (2015). Identification of minimum Rpn4-responsive elements in genes related to proteasome functions. FEBS Lett. 589, 933–940. 10.1016/j.febslet.2015.02.025. [PubMed: 25747386]

Sledz P, Unverdorben P, Beck F, Pfeifer G, Schweitzer A, Forster F, and Baumeister W (2013). Structure of the 26S proteasome with ATP-γS bound provides insights into the mechanism of nucleotide-dependent substrate translocation. Proc. Natl. Acad. Sci. U. S. A 110, 7264–7269. 10.1073/pnas.1305782110. [PubMed: 23589842]

Smith DM, Chang SC, Park S, Finley D, Cheng Y, and Goldberg AL (2007). Docking of the proteasomal ATPases' carboxyl termini in the 20S proteasome's alpha ring opens the gate for substrate entry. Mol. Cell 27, 731–744. 10.1016/j.molcel.2007.06.033. [PubMed: 17803938]

Sokolova V, Li F, Polovin G, and Park S (2015). Proteasome activation is mediated via a functional switch of the rpt6 C-terminal tail following chaperone-dependent assembly. Sci. Rep 5, 14909. 10.1038/srep14909. [PubMed: 26449534]

Takagi K, Kim S, Yukii H, Ueno M, Morishita R, Endo Y, Kato K, Tanaka K, Saeki Y, and Mizushima T (2012). Structural basis for specific recognition of Rpt1p, an ATPase subunit of 26 S proteasome, by proteasome-dedicated chaperone Hsm3p. J. Biol. Chem 287, 12172–12182. 10.1074/jbc.m112.345876. [PubMed: 22334676]

Teixeira LK, and Reed SI (2013). Ubiquitin ligases and cell cycle control. Annu. Rev. Biochem 82, 387–414. 10.1146/annurev-bio-chem-060410-105307. [PubMed: 23495935]

Thompson D, Hakala K, and DeMartino GN (2009). Subcomplexes of PA700, the 19 S regulator of the 26 S proteasome, reveal relative roles of AAA subunits in 26 S proteasome assembly and activation and ATPase activity. J. Biol. Chem 284, 24891–24903. 10.1074/jbc.m109.023218. [PubMed: 19589775]

Tomko RJ Jr., Funakoshi M, Schneider K, Wang J, and Hochstrasser M (2010). Heterohexameric ring arrangement of the eukaryotic proteasomal ATPases: implications for proteasome structure and assembly. Mol. Cell 88, 393–403. 10.1016/j.molcel.2010.02.035.

Tsvetkov P, Sokol E, Jin D, Brune Z, Thiru P, Ghandi M, Garraway LA, Gupta PB, Santagata S, Whitesell L, and Lindquist S (2017). Suppression of 19S proteasome subunits marks emergence of an altered cell state in diverse cancers. Proc. Natl. Acad. Sci. U. S. A 114, 382–387. 10.1073/pnas.1619067114. [PubMed: 28028240]

Tucker M, Staples RR, Valencia-Sanchez MA, Muhlrad D, and Parker R (2002). Ccr4p is the catalytic subunit of a Ccr4p/Pop2p/Notp mRNA deadenylase complex in Saccharomyces cerevisiae. EMBO J. 21, 1427–1436. 10.1093/emboj/21.6.1427. [PubMed: 11889048]

Tucker M, Valencia-Sanchez MA, Staples RR, Chen J, Denis CL, and Parker R (2001). The transcription factor associated Ccr4 and Caf1 proteins are components of the major cytoplasmic mRNA deadenylase in Saccharomyces cerevisiae. Cell 104, 377–386. 10.1016/s0092-8674(01)00225-2. [PubMed: 11239395]

Unverdorben P, Beck F, Sledz P, Schweitzer A, Pfeifer G, Plitzko JM, Baumeister W, and Foerster F (2014). Deep classification of a large cryo-EM dataset defines the conformational landscape of the 26S proteasome. Proc. Natl. Acad. Sci. U. S. A 111, 5544–5549. 10.2210/pdb4cr4/pdb. [PubMed: 24706844]

Villanyi Z, Ribaud V, Kassem S, Panasenko OO, Pahi Z, Gupta I, Steinmetz L, Boros I, and Collart MA (2014). The Not5 subunit of the ccr4-not complex connects transcription and translation. PLoS Genet. 10, e1004569. 10.1371/journal.pgen.1004569. [PubMed: 25340856]

Wani PS, Rowland MA, Ondracek A, Deeds EJ, and Roelofs J (2015). Maturation of the proteasome core particle induces an affinity switch that controls regulatory particle association. Nat. Commun 6, 6384. 10.1038/ncomms7384. [PubMed: 25812915]

Wehmer M, Rudack T, Beck F, Aufderheide A, Pfeifer G, Plitzko JM, Forster F, Schulten K, Baumeister W, and Sakata E (2017). Structural insights into the functional cycle of the ATPase module of the 26S proteasome. Proc. Natl. Acad. Sci. U. S. A 114, 1305–1310. 10.1073/pnas.1621129114. [PubMed: 28115689]

Xie Y, and Varshavsky A (2001). RPN4 is a ligand, substrate, and transcriptional regulator of the 26S proteasome: a negative feedback circuit. Proc. Natl. Acad. Sci. U. S. A 98, 3056–3061. 10.1073/pnas.071022298. [PubMed: 11248031]

Zavodszky E, Peak-Chew SY, Juszkiewicz S, Narvaez AJ, and Hegde RS (2021). Identification of a quality-control factor that monitors failures during proteasome assembly. Science 373, 998–1004. 10.1126/science.abc6500. [PubMed: 34446601]

Highlights

- Proteasome holoenzyme forms via the assembly checkpoint using dedicated chaperones
- Chaperones at the checkpoint recognize the nucleotide state of proteasomal ATPases
- Specificity of chaperone actions is maintained via their limiting cellular level
- Chaperones promote subunit rearrangement to generate a functional proteasome

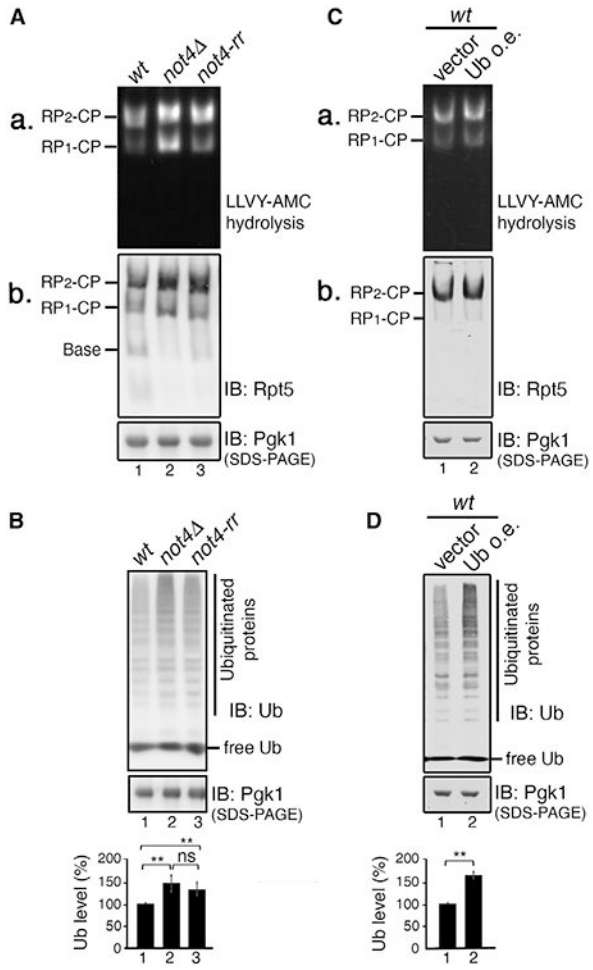

Figure 1. Increased proteasome assembly can result in deficient protein degradation

(A) Increased assembly of the proteasome holoenzyme in *not4* mutants. Native PAGE of whole-cell lysates, followed by LLVY-AMC assay (a) and immunoblotting (b), is shown. IB, immunoblot; Pgk1, loading control in all panels; Rpt5, an RP subunit.

(B) Deficient degradation of ubiquitinated proteins in *not4* mutants. SDS-PAGE and immunoblotting of whole-cell lysates is shown. Quantification is shown in graph (mean ± SD; n = 4 biological replicates; **p < 0.005; ns, not significant).

(C and D) Increased synthesis of ubiquitinated protein does not influence proteasome holoenzyme assembly. Wild-type cells harboring vector or ubiquitin-overexpressing plasmid (Ub o.e.) were examined as in (A) and (B), respectively. Quantification is shown in graph (mean ± SD; n = 3 biological replicates; **p < 0.005).

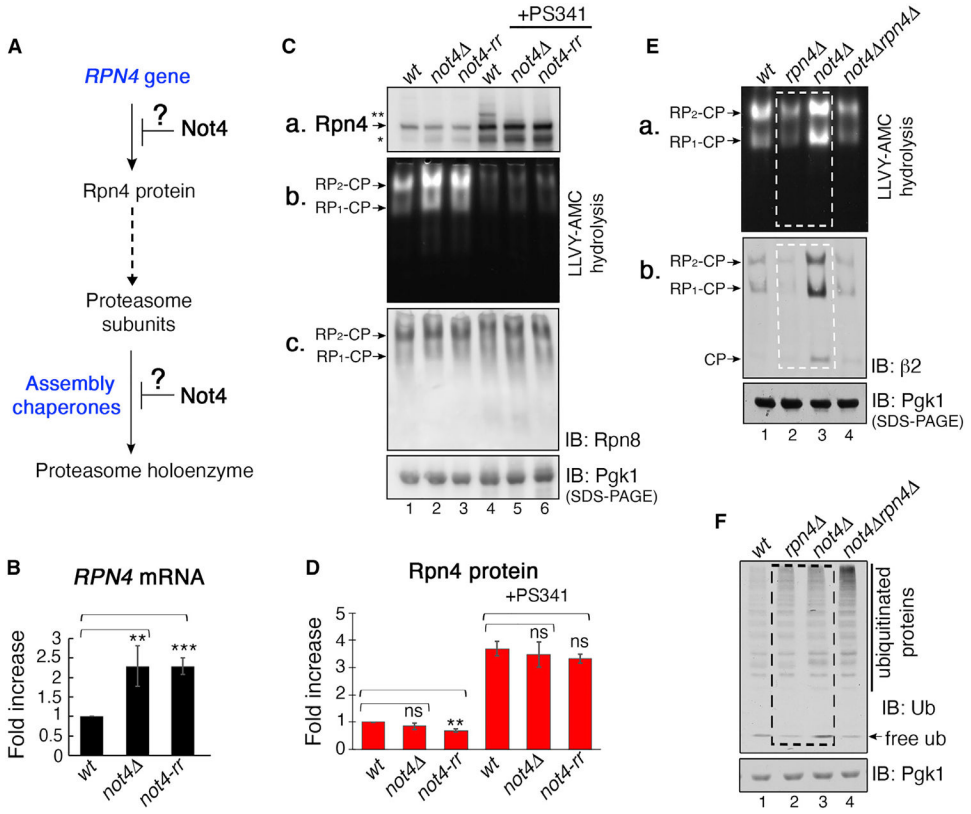

Figure 2. Proteasome assembly is regulated antagonistically via Not4, downstream of Rpn4

(A) Diagram showing proteasome biogenesis via Rpn4 and assembly chaperones and potential steps for antagonistic control via Not4.

(B) Increased *RPN4* mRNA level in *not4* mutants. Quantitative real-time PCR results show *RPN4* mRNA induction (mean ± SD; n = 3 biological replicates; **p < 0.005; ***p < 0.0005).

(C) Comparable Rpn4 protein level between wild type and *not4* mutants. Cells were grown without or with PS341 (40 μM; 3 h) to examine Rpn4 protein level (a) by SDS-PAGE and immunoblotting (**ubiquitinated Rpn4; *partially degraded Rpn4). Proteasome holoenzyme activity and level were assessed by native PAGE followed by LLVY-AMC hydrolysis (b) and immunoblotting (c). Pgk1, loading control in (C), (E), and (F); Rpn8, an RP subunit.

(D) Quantification of Rpn4 protein level from data, as in (Ca) (mean ± SD; n = 4 biological replicates; **p < 0.005).

(E) Not4 regulates proteasome holoenzyme assembly downstream of Rpn4. Experiments were conducted as in (C). β2, a CP subunit.

(F) Impaired degradation of ubiquitinated proteins in *rpn4Δ* and *not4Δ* cells, as assessed by SDS-PAGE and immunoblotting.

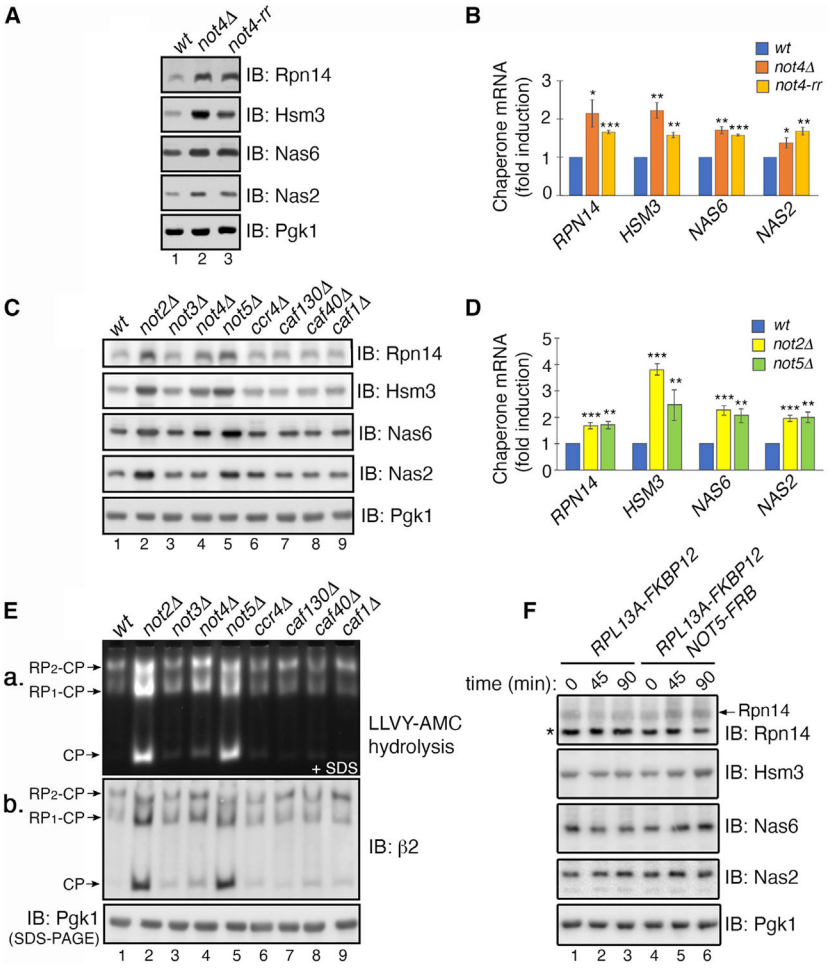

Figure 3. Not4 antagonizes RP chaperone transcription via its NOT module in Ccr4-Not

(A–D) Not4 regulates chaperone protein levels by antagonizing their transcription via the NOT module. SDS-PAGE and immunoblotting of chaperone proteins are shown (A and C). Quantitative real-time PCR shows chaperone mRNA induction (B and D) (mean ± SD; n = 3 biological replicates; *p < 0.05; **p < 0.005; ***p < 0.0005).

(E) NOT module activity contributes to proper assembly of the proteasome holoenzyme. Native-PAGE, followed by LLVY-AMC assay (a) and immunoblotting (b), is shown. 0.02% SDS (a) activates free CP by denaturing its substrate entry gate (Groll et al., 2000).

(F) Conditional inactivation of the NOT module deregulates chaperone levels. Rapamycin (7.5 μM) induces anchor-away of the NOT module (see text for detail). Chaperone levels were examined as in (A). *Non-specific signal.

Pgk1, loading control for (A), (C), (E), and (F).

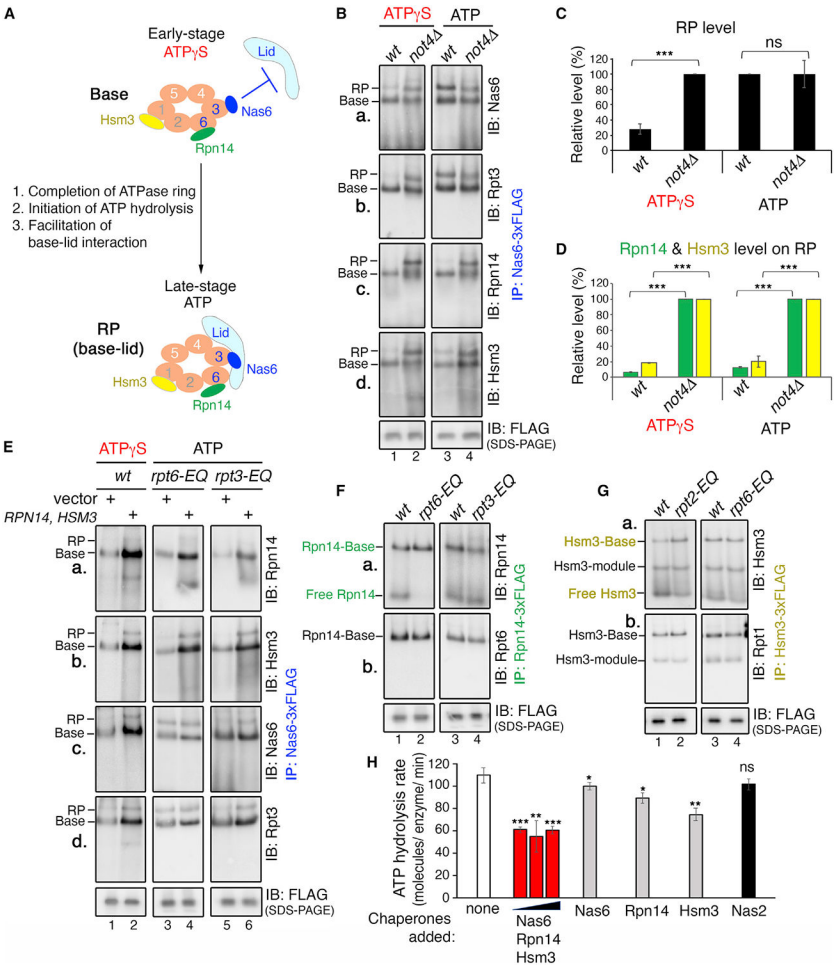

Figure 4. The RP assembly checkpoint requires proper chaperone levels to select an RP base and modulate its ATP hydrolysis for correct base-lid interaction

(A) Cartoon depicting the RP assembly checkpoint and its three proposed steps (see text for details). Nas6 obstructs lid binding (top), until completion of the heterohexameric Rpt ring (orange, Rpt1–6); white, gray, and black fonts indicate three Rpt modules. For simplicity, non-ATPase subunits are omitted. Nas2 is not shown since it releases from the fully formed base (Tomko et al., 2010).

(B) Impaired RP assembly checkpoint in *not4Δ* cells, as suggested by increased RP in an ATPγS condition. Nas6 pull-down in the presence of ATPγS or ATP (1 mM each) was subjected to native gels and immunoblotting (a–d). Anti-FLAG immunoblot, loading control for (B) and (E)–(G); see also Figures S2D-S2G.

(C and D) Quantification of RP level (C) and the RP-bound Rpn14 and Hsm3 level (D), using data as in (Ba) and (Bb) and (Bc) and (Bd), respectively (n = 4 biological replicates; mean ± SD; ***p < 0.0005).

(E) Excess Rpn14 and Hsm3 disrupt the RP assembly checkpoint via saturating the base. Rpn14 and Hsm3 levels were increased using low-copy expression plasmids. Nas6 pull-down was conducted and analyzed as in (B). ATP was used in the *rpt-EQ* cells, since specific Rpt subunits are fixed in the ATP-bound state.

(F and G) Rpn14 and Hsm3 at their normal endogenous expression level can distinguish the ATP-bound state of their cognate Rpt subunits. Experiments were conducted as in (B), in the presence of ATP (1 mM). Hsm3-module (G) indicates Hsm3-Rpt1-Rpt2-Rpn1 complex (Funakoshi et al., 2009; LeTallec et al., 2009; Saeki et al., 2009).

(H) Chaperones influence ATP hydrolysis at the RP assembly checkpoint. Three chaperones were added at a 1-, 2.5-, and 5-fold molar ratio to the wild-type RP (250 nM) or individually at an equimolar ratio to it. The rate of ATP hydrolysis was measured using real-time NADH enzyme-linked assays (mean ± SD; n= 3 biological replicates; *$p < 0.05$; **$p < 0.005$; ***$p < 0.0005$).

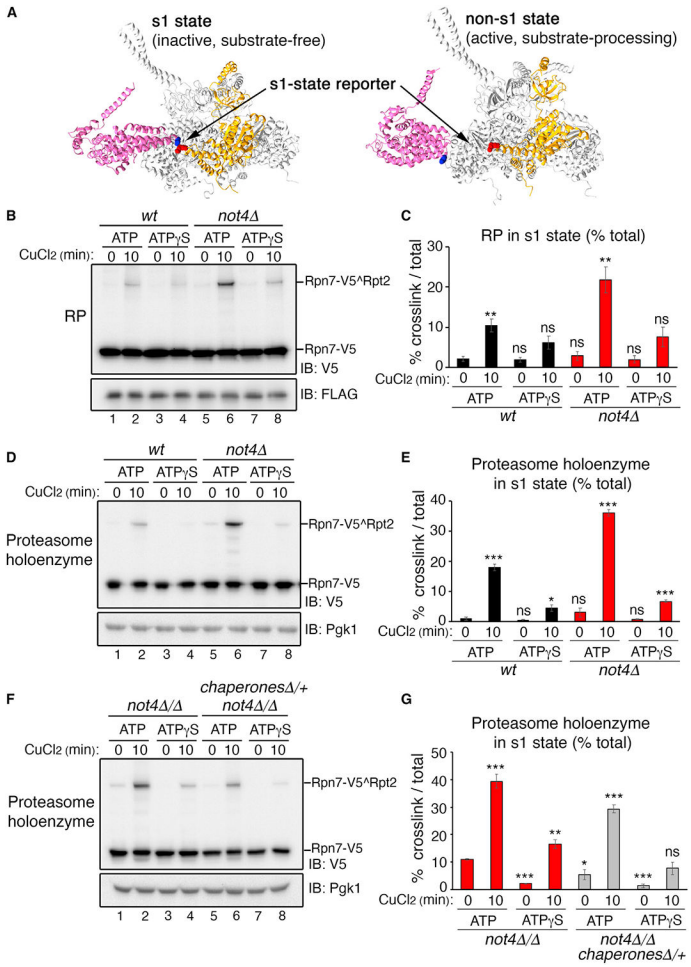

Figure 5. The RP assembly checkpoint facilitates subunit rearrangement for RP remodeling

(A) Conformational changes in the s1 versus non-s1 state of the proteasome holoenzyme. Rpn7-D123 (blue dot) and Rpt2-R407 (red dot) are proximal in the s1 state (PDB: 4CR2), but not in the other states, such as the s3 state (PDB: 4CR4) (Unverdorben et al., 2014); Rpn7 (pink), Rpt2 (orange), and other Rpt subunits (gray) are shown. Non-ATPase subunits are omitted for simplicity.

(B–G) The s1 state (%) is increased in the RP and the resulting proteasome holoenzymes in *not4Δ* cells due to increased chaperone level. Crosslinking was induced using $CuCl_2$ in the presence of ATP or ATPγS (2 mM each) and assessed by SDS-PAGE and immunoblotting for a V5 tag on Rpn7 (B, D, and F). Graphs (C, E, and G) show the % s1 state: (crosslinked signal)/(crosslinked + uncrosslinked signal) (mean ± SD; n = 3 biological replicates; *p < 0.05; **p < 0.005; ***p < 0.0005).

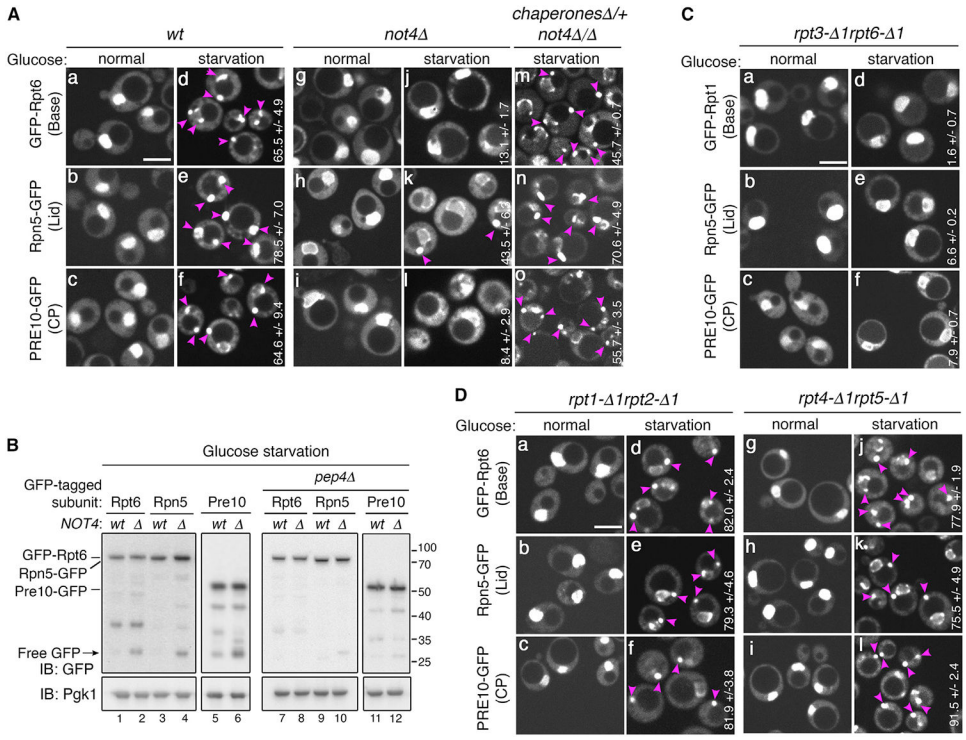

Figure 6. The fate of the proteasome holoenzyme depends on RP remodeling, as ensured by the RP assembly checkpoint

(A) Upon glucose starvation, proteasomal complexes form PSGs (arrowheads) in wild-type, but not in *not4Δ*, cells due to increased chaperone level. For live-cell confocal microscopy, cells were grown to an early log phase with 2% glucose (normal) or for 4 days without glucose (starvation) (Li et al., 2019); % of cells with PSG formation is indicated on the side within each panel. In (m)–(o), *chaperonesΔ/+* indicates *rpn14Δ/+ hsm3Δ/+ nas6Δ/+*. Scale bar, 5 μm.

(B) GFP release assays showing autophagic degradation of proteasomal complexes in *not4Δ* cells. SDS-PAGE and immunoblotting of whole-cell extracts are shown upon glucose starvation as in (A). Molecular weight markers (kDa) are shown at right.

(C and D) Rpt3 and Rpt6 tails are crucial for PSG formation of the proteasomal complexes upon glucose starvation. Experiments were conducted as in (A); % of cells with PSG formation (arrowheads) is indicated on the side within each panel (starvation). Scale bars, 5 μm.

KEY RESOURCES TABLE

REAGENT or RESOURCE	SOURCE	IDENTIFIER
Antibodies		
Mouse monoclonal Anti-Ub	Enzo Life Sciences	BML-PW0930-0100; RRID: AB_11181462
Rabbit polyclonal anti-β2	Dohmen laboratory (Marques et al., 2007)	N/A
Mouse monoclonal Anti-HA-HRP (3F10)	Sigma	12013819001; RRID: AB_390917
Rabbit polyclonal Anti-Rpt1	Carl Mann laboratory (Ghislain et al., 1993)	N/A
Rabbit polyclonal Anti-Rpt3	Enzo Life Sciences	BML-PW8250-0025; RRID: AB_2052357
Rabbit polyclonal Anti-Rpt5	Enzo Life Sciences	BML-PW8245-0100; RRID: AB_10555018
Rabbit polyclonal Anti-Rpt6	Carl Mann laboratory (Ghislain et al., 1993)	N/A
Rabbit polyclonal Anti-Rpn1	Finley laboratory (Shi et al., 2016)	N/A
Rabbit polyclonal Anti-Ubp6	Finley laboratory (Hanna et al., 2006)	N/A
Rabbit polyclonal Anti-Rpn8	Finley laboratory (Roelofs et al., 2009)	N/A
Rabbit polyclonal Anti-Rpn12	Finley laboratory (Roelofs et al., 2009)	N/A
Rabbit polyclonal Anti-Rpn14	Finley laboratory (Roelofs et al., 2009)	N/A
Rabbit polyclonal Anti-Nas6	Finley laboratory (Roelofs et al., 2009)	N/A
Rabbit polyclonal Anti-Hsm3	Finley laboratory (Roelofs et al., 2009)	N/A
Rabbit polyclonal Anti-Nas2	Roelofs Laboratory (Lee et al., 2011)	N/A
Mouse monoclonal Anti-Pgk1	Life Technologies	459250; RRID: AB_2532235
Mouse monoclonal Anti-FLAG	Sigma	F3165; RRID: AB_259529
Mouse monoclonal MCP231	Enzo Life Sciences	BML-PW8195-0100; RRID: AB_11181772
Rabbit polyclonal Anti-Pba1/2	Roelofs Laboratory (Wani et al., 2015)	N/A
Anti-Mouse IgG, HRP-linked secondary antibody	Cytiva	NA931-1ML; RRID: AB_772210
Anti-Rabbit IgG, HRP-linked secondary antibody	Cytiva	NA934-1ML; RRID: AB_772206
Bacterial and virus strains		
Rosetta2 (DE3) competent cells	Millipore Sigma	713974
Chemicals, peptides, and recombinant proteins		
LLVY-AMC	Bachem	I-1395.0100
Rapamycin	LC laboratories	R5000
PS-341	LC laboratories	B1408
ATP	Sigma	A3377-25G

REAGENT or RESOURCE	SOURCE	IDENTIFIER
ATPγS	Sigma	A1388-25MG
Anti-FLAG M2 affinity gel	Sigma	A2220-5ML
3X FLAG Peptide	GLP Bio	GP10149-5
Sypro Ruby	Invitrogen	S12001
Reverse transcriptase (IMPROM-II)	Promega	PRA3802
IQ SYBR Green Supermix	Bio-Rad	1708882
IgG Affinity Gel	MP Biomedicals	ICN55961
TEV protease	Promega	PRV6101
Glutathione Sepharose beads	Cytiva	17513201
PreScission Protease	GenScript	Z02799-250
Experimental models: Organisms/strains		
S. cerevisiae strain SUB62	Finley et al., 1987	N/A
For isogenic mutants of SUB62 used herein, see Table S2.	This study	N/A
Oligonucleotides		
qRT-PCR primer for *RPN4*: forward, CCGTCTACTGCTACTACCGG	This study	N/A
qRT-PCR primer for *RPN4*: reverse, CCGCCTACTAGCATTTGAGC	This study	N/A
qRT-PCR primer for *RPN14*: forward, CGACACCAGTATTAAGCTTGACATTAT	Shirozu et al., 2015	N/A
qRT-PCR primer for *RPN14*: reverse, TGGGCGTCTCAAATTCAATAG	Shirozu et al., 2015	N/A
qRT-PCR primer for *HSM3*: forward, AAAATTTCTGCTCAATGAGATGC	Shirozu et al., 2015	N/A
qRT-PCR primer for *HSM3*: reverse, GCGCTCCCATCACCTATC	Shirozu et al., 2015	N/A
qRT-PCR primer for *NAS6*: forward, TGGTGCAGAATATGATCTTGTAGATA	Shirozu et al., 2015	N/A
qRT-PCR primer for *NAS6*: reverse, TTAACCTGTTCATTAAGGGCAAC	Shirozu et al., 2015	N/A
qRT-PCR primer for *NAS2*: forward, CTAGAGGCGTATTTCAGTGTGC	Shirozu et al., 2015	N/A
qRT-PCR primer for *NAS2*: reverse, TCACCAACGCAGAGTCCAT	Shirozu et al., 2015	N/A
qRT-PCR primer for *ACT1*: forward, CCATCTTCCATGAAGGTCAAG	Shirozu et al., 2015	N/A
qRT-PCR primer for *ACT1*: reverse, CCACCAATCCAGACGGAGTA	Shirozu et al., 2015	N/A
Recombinant DNA		
For plasmids used herein, see Table S3.	This study	N/A
Software and algorithms		
UCSF Chimera	Pettersen et al., 2004	http://www.cgl.ucsf.edu/chimera/
ImageJ	Schneider et al., 2012	https://imagej.nih.gov/ij/